# Chapter 3: Construction and Application of a Rh-Pt DNA Metalloinsertor Conjugate*

## 3.1 Introduction

Platinum anti-cancer compounds are among the most successful and most widely used chemotherapeutic agents to date.[1] By forming covalent adducts with the DNA bases, platinum chemotherapeutics cause lesions that inhibit transcription and DNA repair, leading to apoptosis.[2] However, while cisplatin and carboplatin have been highly successful in the treatment of testicular, cervical, ovarian, and non-small cell lung cancers, their use is limited by severe side effects and resistance.[2,3] Specifically, cancers that exhibit deficiencies in the mismatch repair (MMR) machinery are largely resistant to cisplatin treatment, as MMR proteins are among those responsible for the recognition of Pt-DNA lesions.[4,5] MMR-deficient cancers, which comprise 15% of sporadic colorectal cancer cases and 18% of all solid tumors, can be treated in part with oxaliplatin, which employs a *trans* 1,2-diaminocyclohexane non-leaving group ligand instead of the amines.[6-8] As a result, oxaliplatin-DNA adducts are poorly recognized by MMR proteins, rendering the drug highly effective against cisplatin-resistant cancers *in vitro*.[8] However, the efficacy of oxaliplatin *in vivo* is severely limited, and treatment must be administered in combination with a variety of drugs, such as 5-fluorouracil and leucovorin.[8,9] Although this combinatorial approach does increase the response rate of oxaliplatin treatment, the improvement is modest, and the overall efficacy in the later stages of colorectal cancer is still very low.

---

*Adapted from Weidmann, A. G.; Barton, J. K. *Inorg. Chem.* **2014**, *53*, 7812-7814.

Rhodium metalloinsertors may offer a promising strategy in the development of new therapies for such cancers. These bulky, octahedral rhodium (III) complexes bind specifically to DNA base pair mismatches,[10] which are amplified in cells with defective MMR machinery.[6,7] This selectivity is achieved through *metalloinsertion*, a general binding mode in which a sterically expansive ligand inserts into the base stack at the site of the thermodynamically destabilized mismatch, ejecting the mismatched bases from the duplex.[11-13] It is postulated that this large lesion created upon rhodium mismatch binding is recognized *in cellulo*, leading to a selective cellular response. Metalloinsertors exhibit cytotoxicity preferentially in MMR-deficient cells, and the extent of this selectivity correlates with mismatch binding affinity and localization to the nucleus, where they target mismatches in genomic DNA.[14-17]

The design of bifunctional drug conjugates is a burgeoning field in chemotherapy, especially as a strategy to circumvent resistance.[18] Here, we present a bimetallic oxaliplatin-metalloinsertor conjugate (RhPt), that displays dual DNA binding behavior *in vitro*. Additionally, RhPt exhibits enhanced cytotoxicity and cellular uptake in MMR-deficient HCT116O human colorectal cancer cells compared to first-line platinum therapeutics therapeutics as well as its unconjugated subunits. The cytotoxicity of RhPt appears to be triggered by an apoptotic cell death pathway, and its potency is attributed to the improved cellular uptake of the complex.

## 3.2 Experimental Protocols

### 3.2.1 Materials

A2780cis cells, cisplatin, oxaliplatin, and all organic reagents were purchased from Sigma-Aldrich unless otherwise noted. Commercially available chemicals were

used as received without further purification. $RhCl_3$ and $K_2PtCl_4$ starting material were purchased from Pressure Chemical Co (Pittsburgh, PA). Sep-pak $C_{18}$ solid-phase extraction (SPE) cartridges were purchased from Waters Chemical Co. (Milford, MA). Media and supplements were purchased from Invitrogen (Carlsbad, CA). BrdU, antibodies, and buffers were purchased in kit format from Roche Molecular Biochemical (Mannheim, Germany). Simian virus 40 (SV40) T-large antigen, origin-containing pUC HSO plasmid DNA, HeLa cell extract, and all buffers and reagents for the SV40 DNA replication assay were purchased in kit format from CHIMERx (Milwaukee, WI).

Oligonucleotides were ordered from Integrated DNA Technologies and purified by HPLC using a C18 reverse-phase column (Varian, Inc; Corona, CA). All HPLC purifications were carried out on a Hewlett-Packard 1100 HPLC. DNA purity was confirmed by MALDI-TOF mass spectrometry and quantified by UV-visible spectroscopy (UV-vis) using the extinction coefficients at 260 nm estimated for single-stranded DNA. UV-vis characterizations were performed on a Beckmann DU 7400 spectrophotometer. Radiolabeled [$^{32}$P]-ATP was purchased from MP Biomedicals (Santa Ana, CA).

The syntheses of chrysene-5,6-dione (chrysi), $[Pt(DACH)(H_2O)_2]SO_4$ (*DACH* = (1*R*,2*R*)-(-)-1,2-diaminocyclohexane), and di(pyridin-2-yl)glycine (dpa-AcOH*)* were carried out according to published procedures.[19-21] The synthesis of precursor $[Rh(chrysi)(HDPA)(NH_3)_2]TFA_3$ was carried out in a manner analogous to that of $[Rh(chrysi)(phen)(NH_3)_2]$, as described by Mürner et al.[19]

### 3.2.2 Synthesis of Rhodium Scaffold Precursor (Scheme 3.1)

#### 3.2.2.1 $[Rh(HDPA)Cl_4]HDPA$ (*6*)

[Rh(HDPA)$Cl_4$]HDPA (HDPA = 2,2'-dipyridylamine) was prepared according to a modified literature protocol.[19] $RhCl_3 \bullet H_2O$ (1.9 g, 8.4 mmol) was suspended in concentrated HCl (30 ml) and refluxed for 4 h. To the dark red solution was added HDPA (1.3 g, 7.56 mmol), followed by the addition of boiling Milli-Q water (250 ml). The orange suspension was refluxed for an additional 16 h and left to stand at 4 °C. The resulting orange precipitate was filtered and washed with ethanol and diethyl ether. Yield: 2.5 g (81%). $^1$H NMR (500 MHz, DMSO-d6) $\delta$ 11.13 (s, 1H), 9.08 – 9.05 (m, 1H), 8.46 (dd, $J$ = 6.2, 1.6 Hz, 1H), 7.88 (dddd, $J$ = 28.2, 8.6, 7.3, 1.7 Hz, 2H), 7.19 (ddd, $J$ = 7.3, 6.2, 1.4 Hz, 1H), 7.13 (dd, $J$ = 8.4, 1.3 Hz, 1H), 7.06 (td, $J$ = 7.6, 1.4 Hz, 2H), 6.82 (s, 2H).

#### 3.2.2.2 [Rh(HDPA)$(OTf)_4$]HDPA (*5*)

[Rh(HDPA)$Cl_4$]HDPA (2.46 g, 4.19 mmol) was dissolved in neat triflic acid (10 g, 66.67 mmol) under argon at ambient temperature. The dark red solution was stirred at room temperature for 16 h, with occasional purging to release HCl gas. The solution was poured over cold diethyl ether (-78 °C), and the brown precipitate was collected by vacuum filtration. Yield: 3.58 g (82 %) $^1$H NMR (500 MHz, DMSO-d6) $\delta$ 8.59 (m, 2H), 8.02 (m, 2H), 7.25 (m, 4H).

#### 3.2.2.3 [Rh(HDPA)$(NH3)_4$]$(OTf)_3$

[Rh(HDPA)$(OTf)_4$]HDPA (3.55 g, 3.39 mmol) was dissolved in concentrated aqueous ammonium hydroxide (100 ml) and refluxed for 45 min. The yellow solution was cooled to room temperature, and the solvent was removed *in vacuo*. The yellow solid was dissolved in a minimum amount of $H_2O$ and triturated with 1:1 EtOH/$Et_2O$. The white precipitate was filtered to give [Rh(HDPA)$(NH_3)_4$]$OTf_3$ as an off-white powder.

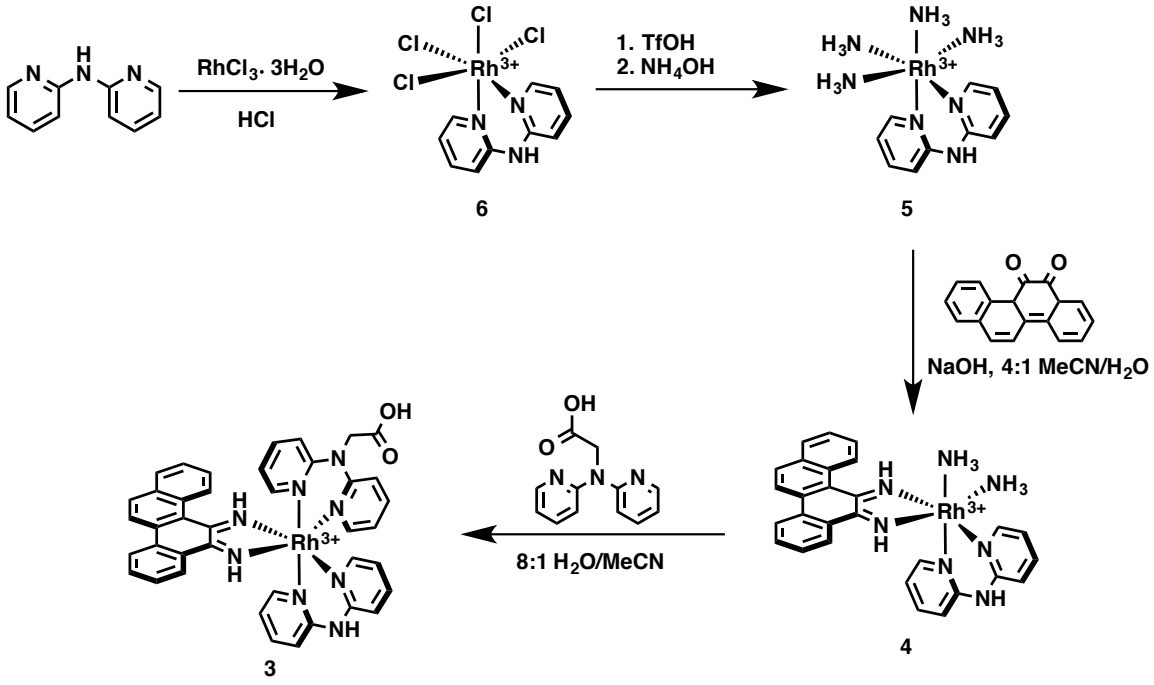


**Scheme 3.1** Synthesis of rhodium metalloinsertor scaffold for conjugation, $[Rh(chrysi)(HDPA)(dpa\text{-}AcOH)]^{3+}$ (**3**).

Yield: 2.0 g (69 %). $^1$H NMR (500 MHz, DMSO-d6): $\delta$ 8.67 (d, $J$ = 5.5 Hz, 1H), 8.29 (d, $J$ = 34.8 Hz, 1H), 7.97 (ddd, $J$ = 32.5, 18.2, 8.1 Hz, 3H), 7.50 – 7.40 (m, 2H), 7.23 (t, $J$ = 5.7 Hz, 1H), 7.15 (t, $J$ = 6.6 Hz, 1H), 4.69 (d, $J$ = 10.0 Hz, 3H), 4.43 (s, 3H), 4.20 – 4.04 (m, 6H).

#### 3.2.2.4 [Rh(HDPA)(chrysi)(NH3)$_2$](TFA)$_3$ (*4*)

[Rh(HDPA)(NH3)$_4$](OTf)$_3$ (2.0 g, 2.3 mmol) and chrysene-5,6-dione (chrysi, 0.66 g, 2.6 mmol) were dissolved in acetonitrile (130 ml). Aqueous sodium hydroxide (1N, 13 ml) was added, and the reaction was allowed to stir at ambient temperature for 16 h. The reaction was neutralized with 1N HCl and dried *in vacuo*. The residue was dissolved in water, desalted on a SPE cartridge (1:1:0.1 $H_2O$:MeCN:TFA), and dried again *in vacuo* to afford a mixture of the two *cis* diastereomers of [Rh(HDPA)(chrysi)($NH_3$)$_2$](TFA)$_3$ as a bright red solid. Yield: 0.62 g (30%). $^1$H NMR (500 MHz, DMSO-d6): $\delta$ $^1$H NMR (500 MHz, DMSO-d6) δ 11.67 (s, 1H), 11.56 (d, $J$ = 2.9 Hz, 1H), 9.09 (dd, $J$ = 6.3, 1.6 Hz, 1H), 8.52 – 8.43 (m, 2H), 8.43 – 8.36 (m, 2H), 8.36 – 8.25 (m, 2H), 8.18 (td, $J$ = 8.0, 7.4, 3.0 Hz, 3H), 8.13 (dd, $J$ = 8.6, 5.6 Hz, 1H), 8.10 (dd, $J$ = 7.8, 1.3 Hz, 1H), 8.08 – 8.03 (m, 2H), 7.99 (dtd, $J$ = 8.5, 7.2, 1.6 Hz, 3H), 7.89 (ddd, $J$ = 8.5, 7.0, 1.5 Hz, 1H), 7.74 (d, $J$ = 8.3 Hz, 1H), 7.71 – 7.67 (m, 1H), 7.66 – 7.61 (m, 2H), 7.61 – 7.57 (m, 2H), 7.54 (td, $J$ = 7.5, 0.9 Hz, 1H), 7.52 – 7.45 (m, 3H), 7.44 (d, $J$ = 1.3 Hz, 1H), 7.44 – 7.41 (m, 2H), 7.40 (d, $J$ = 1.4 Hz, 1H), 7.32 (ddddt, $J$ = 10.3, 6.1, 4.3, 3.0, 1.6 Hz, 3H), 7.27 – 7.20 (m, 2H), 6.98 – 6.95 (m, 1H), 6.95 – 6.89 (m, 2H), 4.68 (d, $J$ = 18.2 Hz, 6H), 4.49 (d, $J$ = 6.3 Hz, 6H), 4.35 (s, 6H). ESI-MS (cation): *m/z* calc 562.48 (M – 2H$^+$), obs. 528.0 (M – 2H – 2$NH_3^+$), 580.8 (M – 2H + $H_2O^+$), 587 (M + $Na^+$).

#### 3.2.2.5 [Rh(HDPA)(chrysi)(dpa-AcOH](TFA)$_3$ (*3*)

[Rh(HDPA)(chrysi)$(NH3)_2$]$(TFA)_3$ (620 mg, 0.69 mmol) and di(pyridin-2-yl)glycine (dpa-AcOH) (240 mg, 1.05 mmol) were dissolved in 8:1 $H_2O$:MeCN (90 ml) and refluxed for 24 h. The solvent was removed *in vacuo*, and the crude product was purified by HPLC using a $C_{18}$ reverse-phase column (Varian, Inc.) on a Hewlett Packard 1100 HPLC (85:15 to 40:60 $H_2O$ (0.1 % TFA):MeCN). Complex **3** was isolated as a dark red, hygroscopic solid. Yield: 0.55 g (73%). $^1$H NMR (300 MHz, DMSO-d6) $\delta$ 11.47 (broad s, 1H), 9.64 (s, 1H), 9.04 (d, $J$ = 6.2 Hz, 1H), 8.77 (dd, $J$ = 15.0, 6.8 Hz, 1H), 8.52 (d, $J$ = 6.1 Hz, 1H), 8.24 (dd, $J$ = 5.0, 1.8 Hz, 4H), 8.08 (dt, $J$ = 16.7, 9.5 Hz, 2H), 8.01 – 7.84 (m, 4H), 7.80 – 7.74 (m, 1H), 7.71 (d, $J$ = 8.1 Hz, 1H), 7.67 (s, 1H), 7.56 – 7.40 (m, 3H), 7.38 – 7.29 (m, 1H), 7.19 (t, $J$ = 8.4 Hz, 4H), 6.99 – 6.86 (m, 3H), 6.86 – 6.74 (m, 1H), 4.63 (s, 2H). ESI-MS (cation): *m/z* calc 757.17 ($M - 2H^+$), 379.59 ($M - H^{2+}$), obs. 756.9, 379.1.

### 3.2.3 Synthesis of Rh(Amal) and RhPt (Scheme 3.2)

#### 3.2.3.1 [Rh(HDPA)(chrysi)(diethyl-2-(2-(di(pyridin-2-yl)amino)acetamido)malonate] $(TFA)_3$

[Rh(HDPA)(chrysi)(dpa-AcOH](TFA)$_3$ (***3***) (100 mg, 0.09 mmol), diethyl aminomalonate hydrochloride (38 mg, 0.18 mmol), and (dimethylamino)-*N*,*N*-dimethyl(3*H*-[1,2,3]triazolo[4,5-*b*]pyridin-3-yloxy)methaniminium hexafluorophosphate (HATU, 83 mg, 0.22 mmol) were combined in a vial and dried under vacuum to remove all water. The solids were dissolved in anhydrous DMF (1.3 ml) under argon and stirred at room temperature for 10 min. Ethyldiisopropylamine (DIPEA, 95 µl, 0.54 mmol) was added, and the solution was allowed to stir at room temperature for 12 h. The solvent was removed *in vacuo*, and the intermediate was purified by HPLC as described above. Yield:

41 mg (36% by HPLC). ESI-MS (cation): *m/z* calc 914.24 ($M - 2H^+$), 457.12 ($M - H^{2+}$), obs. 913.9, 457.8

#### 3.2.3.2 [Rh(HDPA)(chrysi)(2-(2-(di(pyridin-2-yl)amino)acetamido)-3-ethoxy-3-oxopropanoic acid)] $(TFA)_3$ ("Rh(Amal")) (*2*)

To hydrolyze the ethyl esters, [Rh(HDPA)(chrysi)(diethyl-2-(2-(di(pyridin-2-yl)amino)acetamido)malonate]$(TFA)_3$ (41 mg, 0.033 mmol) was dissolved in a 5:1 $H_2O$:EtOH mixture (12 ml). 1N NaOH was added to pH 10, and the reaction was stirred at room temperature for 24 h. The solvent was removed by rotary evaporation, and complex **2** ("Rh(Amal)") was purified by HPLC as described above. The chloride salt was obtained from a Sephadex QAE anion-exchange column equilibrated with 0.1 M $MgCl_2$. Yield: 12 mg (30% by HPLC). $^1$H NMR (500 MHz, $D_2O$): $\delta$ 8.91 (dd, $J$ = 6.2, 1.6 Hz, 1H), 8.23 – 8.15 (m, 1H), 8.14 – 8.11 (m, 2H), 8.08 (dd, $J$ = 13.5, 7.6 Hz, 1H), 8.00 (ttd, $J$ = 8.3, 6.9, 1.8 Hz, 3H), 7.94 – 7.90 (m, 1H), 7.90 – 7.85 (m, 1H), 7.83 (d, $J$ = 7.6 Hz, 1H), 7.79 (d, $J$ = 1.7 Hz, 1H), 7.78 – 7.76 (m, 1H), 7.59 (ddd, $J$ = 7.9, 6.5, 1.3 Hz, 1H), 7.51 – 7.45 (m, 3H), 7.36 (td, $J$ = 6.9, 6.3, 1.4 Hz, 2H), 7.34 – 7.30 (m, 1H), 7.29 (d, $J$ = 1.2 Hz, 1H), 7.27 (ddd, $J$ = 4.6, 2.4, 1.0 Hz, 1H), 7.26 (q, $J$ = 2.2 Hz, 1H), 7.25 – 7.22 (m, 1H), 7.21 – 7.17 (m, 1H), 7.11 – 7.06 (m, 3H), 6.91 (ddd, $J$ = 7.7, 6.5, 1.4 Hz, 1H), 4.87 (s, 2H), 3.67 (s, 1H). ESI-MS (cation): *m/z* calc 858.18 ($M - 2H^+$), 429.09 ($M - H^{2+}$), obs. 857.7, 429.5. UV-vis ($H_2O$, pH 7): 259 nm (53,500 $M^{-1}$ $cm^{-1}$), 287 nm (39,300 $M^{-1}$ $cm^{-1}$), 402 nm (6,400 $M^{-1}$ $cm^{-1}$).

#### 3.2.3.3 "RhPt"

To a solution of Rh(Amal) (12 mg, 0.01 mmol) in $H_2O$ (10 ml) was added aqueous $Ba(OH)_2 \bullet 8H_2O$ (54 mg, 0.17 mmol in 5 ml $H_2O$) to pH 11. The yellow

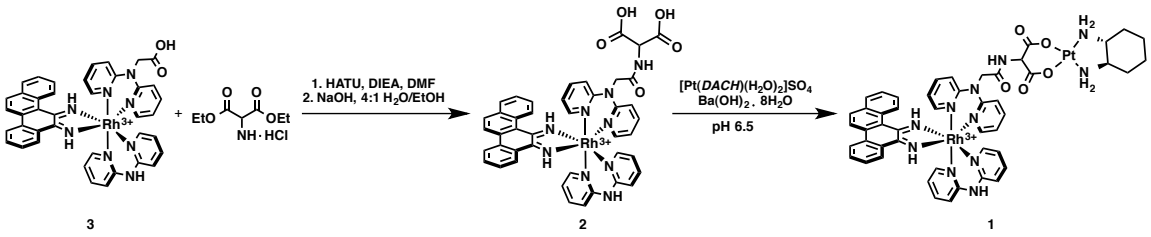


**Scheme 3.2** Synthesis of conjugate "RhPt" (**1**), and its immediate precursor "Rh(Amal)" (**2**). Conjugate **1** is synthesized from **2** via chelation of the platinum subunit [Pt(*DACH*)($H_2O$)$_2$]$SO_4$ (*DACH* = (1*R*,2*R*)-(-)-1,2-diaminocyclohexane) to the dicarboxylate moiety on the metalloinsertor.

suspension was sonicated and added dropwise to a stirred solution of $[Pt(DACH)(H_2O)_2]SO_4$ (76 mg, 0.17 mmol) in $H_2O$ (10 ml) at ambient temperature. The solution turned orange upon addition of the Ba/Rh mixture, and $BaSO_4$ crashed out as a white precipitate. The remaining $Ba(OH)_2 \bullet H_2O$ stock was added to the mixture until pH 7 was reached, and the reaction was allowed to stir at room temperature for 24 h. The $BaSO_4$ byproduct was filtered, and the filtrate was concentrated *in vacuo* and purified by HPLC. The chloride salt was obtained from a Sephadex QAE anion-exchange column equilibrated with 0.1 M $MgCl_2$. Yield: 7.1 mg (57% by HPLC). $^1$H NMR (300 MHz, $D_2O$): $\delta$ 10.06 (s, 1H, chrysi NH), 8.19 (d, $J$ = 6.9 Hz, 1H, chrysi CH), 8.12 (d, $J$ = 13.2 Hz, 1H, chrysi CH), 8.05 (d, $J$ = 9.2 Hz, 1H, chrysi CH), 8.00 – 7.92 (m, 1H, chrysi CH), 7.89 (d, $J$ = 10.0 Hz, 1H, chrysi CH), 7.83 (s, 1H, chrysi CH), 7.80 (s, 1H, chrysi CH), 7.74 (s, 1H, CONH), 7.64 (d, $J$ = 8.1 Hz, 2H, py), 7.55 (d, 1H, chrysi CH), 7.54 – 7.47 (m, 2H, py), 7.47 – 7.33 (m, 1H, chrysi CH), 7.23 (d, $J$ = 6.1 Hz, 1H, chrysi CH), 7.13 (dt, $J$ = 13.3, 6.5 Hz, 2H, py), 6.97 (dd, $J$ = 14.5, 7.1 Hz, 2H, py), 6.42 – 5.93 (m, 2H, Pt-$NH_2$), 5.57 – 5.03 (m, 2H, Pt-$NH_2$), 2.43 (d, $J$ = 1.3 Hz, 2H, dach CH), 1.92 (d, $J$ = 10.1 Hz, 1H, dach CH), 1.43 (s, 2H, dach CH), 1.16 (s, 1H, dach CH), 0.99 (t, $J$ = 10.2 Hz, 2H, dach CH). ESI-MS (cation): *m/z* calc 1165.24 ($M - 2H^+$), 583.12 ($M - H^{2+}$), obs. 1165.9, 582.9. UV-vis ($H_2O$, pH 7): 315 nm (27,000 $M^{-1}$ $cm^{-1}$), 389 nm (5,420 $M^{-1}$ $cm^{-1}$).

### 3.2.4 [Pt(DACH)(aminomalonate)] ("Pt(Amal)," Scheme 3.3)

Diethyl aminomalonate hydrochloride (110 mg, 0.52 mmol) was hydrolyzed in a solution of 4:1 $H_2O$:EtOH (10 ml) basified with 1N NaOH (pH 13). The reaction was stirred at room temperature overnight, neutralized with 1N HCl, and dried *in vacuo* to afford the diacid as a white solid. The resulting aminomalonic acid hydrochloride (78 mg,

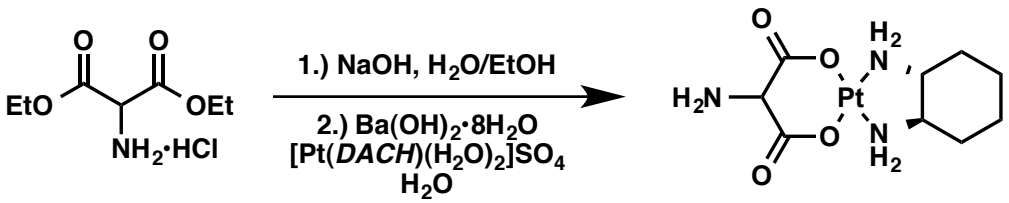


**Scheme 3.3** Synthesis of platinum subunit, "Pt(Amal)."

0.366 mmol) was added to a suspension of $Ba(OH)_2 \bullet 8H_2O$ (58 mg, 0.183 mmol) in 10 ml $H_2O$. The mixture was added dropwise to a solution of $[Pt(DACH)(H_2O)_2]SO_4$ (81 mg, 0.183 mmol) in $H_2O$ (20 ml) and stirred at room temperature, pH 7, for 3h. The $BaSO_4$ precipitate was removed by vacuum filtration, and the filtrate was left to stand at 4 °C. A yellow precipitate was filtered and dried under vacuum. The residue was dissolved in a minimum volume of water, filtered through Celite, and dried under vacuum again to give Pt(Amal) as a pale yellow solid. Yield: 10 mg (13%). $^1$H NMR (300 MHz, $D_2O$): 3.96 (s, 2H), 3.74 (s, 1H), 2.26 (m, 2H), 1.98 (m, 2H), 1.40 (m, 2H), 1.31 (m, 2H), 0.99 (m, 2H). ESI-MS (cation): *m/z* calc 426.09, obs. 449.0 ($M + Na^+$).

### 3.2.5 Photocleavage Competition Titrations

A single-stranded DNA oligomer with the sequence 5'-TTAGGATCATCCATATA-3' (underline denotes the mismatch) was labeled at the 5'-end with [$^{32}$P]-ATP using polynucleotide kinase (PNK) at 37 °C for 1 h. The radiolabeled DNA was purified by gel electrophoresis. A small amount of labeled DNA (less than 1% of the total amount of DNA) was annealed to either its mismatched complement (containing a CC mismatch) or a fully matched complement by heating to 90 °C in buffer (100 mM NaCl, 20 mM $NaP_i$, pH 7.1), followed by slow cooling to ambient temperature over 3 h, to give a final concentration of 2 μM duplex DNA. Racemic solutions of the RhPt conjugate were prepared in Milli-Q water over a range of concentrations (100 nM – 50 μM). For each sample, 4 μM *rac*-$[Rh(bpy)_2chrysi]Cl_3$ (5 μl), which photocleaves DNA at mismatched sites, 2 μM annealed mismatched duplex DNA (10 μl), and the non-photocleaving RhPt at various concentrations (5 μl) were combined to give 1 μM *rac*-$[Rh(bpy)_2chrysi]Cl_3$ and 1 μM duplex DNA as the final concentrations. A "light" control,

(ØRh, ØPt) consisting of 2 μM DNA mixed with 10 μl Milli-Q water, and a "dark" control (Ø *hυ*), containing the DNA mixed with the highest concentration of RhPt without irradiation, were also prepared. The samples were vortexed and, except for the dark control, irradiated on an Oriel (Darmstadt, Germany) 1000-W Hg/Xe solar simulator (340-440 nm) for 15 min. The samples were then incubated at 37 °C for 10 minutes to degrade any metastable products and dried under vacuum. The irradiated samples were electrophoresed on a 20% denaturing polyacrylamide gel and exposed to a phosphor screen. The amounts of DNA in each band were analyzed by autoradiography and quantitated by phosphorimagery (ImageQuant).

### 3.2.6 Binding Constant Determination

As the RhPt complex does not photocleave DNA upon irradiation, the binding affinity for a CC mismatch was determined *via* a competition titration against *rac*-$[Rh(bpy)_2chrysi]^{3+}$, which does photocleave DNA at mismatched sites. To assess the binding of the rhodium subunit of RhPt at the CC mismatch, the fraction of cleaved DNA was quantified and expressed as a percentage of the total DNA in each lane and plotted against the log of the concentration of RhPt. The data from three independent titration experiments were each fit to a sigmoidal curve using OriginPro 8.5. The concentration of rhodium at the inflection point at the curve ($[Rh_{50\%}]$) was then used to solve simultaneous equilibria involving DNA, $[Rh(bpy)_2chrysi]Cl_3$, and RhPt in Mathematica 8.0 to obtain the binding constant ($K_B$).

DNA platination was analyzed in a similar manner, wherein the fraction of platinated DNA was quantified and expressed as a percentage of the total DNA in each

lane and plotted against the log of the concentration of RhPt. The data from three independent titrations were each plotted in OriginPro 8.5.

### 3.2.7 Dimethyl Sulfate Footprinting of Platinated DNA

DNA footprinting of guanine by dimethyl sulfate (DMS) was carried out according to literature procedures.[22] Briefly, single stranded DNA with the sequence 5'-TTAGGATCATCCATATA-3' (underline denotes the mismatch) was labeled at the 5'-end with [$^{32}$P]-ATP and annealed with its CC mismatched complement as described above. A solution of 1 μM annealed DNA was platinated with either RhPt or oxaliplatin at the concentrations indicated by incubation at 37 °C for 90 min. After cooling to 25 °C, the samples were dried *in vacuo* and taken up in 5 μl Milli-Q water. The samples were diluted with DMS buffer (50 mM sodium cacodylate, 1 mM EDTA, pH 7.5), and 2 mM calf-thymus DNA (4 μl) was added as a carrier. Samples were cooled to 0 °C and treated with 5 μl DMS (10% v/v in EtOH) for 5 min at 25 °C. The reaction was quenched *via* addition of the DMS stop solution (1.5 M NaOAc, 1 M β-mercaptoethanol, 250 μg/ml yeast tRNA) at 0 °C. Following ethanol precipitation of the DNA, samples were treated with 10% aqueous piperidine and heated to 90 °C for 30 min. The piperidine was removed *in vacuo*, and samples were electrophoresed on a 20% denaturing polyacrylamide gel and exposed to a phosphor screen. The amounts of DNA in each band were analyzed by autoradiography and quantitated by phosphorimagery (ImageQuant).

### 3.2.8 Cell Culture

**3.2.8.1 HCT116N/O**. HCT116N (MMR-proficient) and HCT116O (MMR-deficient) cells were grown in RPMI medium 1640 supplemented with 10% fetal bovine serum, 400 μg/ml Geneticin (G418), 2 mM L-glutamine, 0.1 mM nonessential

amino acids, 1 mM sodium pyruvate, 100 units/ml penicillin, and 100 μg/ml streptomycin. Cells were grown in tissue culture flasks (Corning Costar, Acton, MA) at 37 °C under a humidified atmosphere (5% $CO_2$).

**3.2.8.2 A2780cis**. A2780cis cells (Sigma-Aldrich Co.) were grown in RPMI medium 1640 supplemented with 105 fetal bovine serum, 200 mM L-glutamine, 100 units/ml penicillin, and 100 μg/ml streptomycin. To retain resistance, cisplatin was added to the media every 2-3 passages to a final concentration of 1 μM. Cells were grown in tissue culture flasks (Corning Costar, Acton, MA) at 37 °C under a humidified atmosphere (5% $CO_2$).

### 3.2.9 Cellular Proliferation ELISA

The antiproliferative effects of conjugate RhPt, oxaliplatin, cisplatin, Rh(Amal) and Pt(Amal) were studied *via* enzyme-linked immunosorbent assay (ELISA).[23] HCT116N and HCT116O cells were plated in 96-well plates at 2000 cells/well and given 24 h to adhere. The cells were incubated with varying concentrations of metal complex (0 – 2 μM) and grown for an additional 24 h. In the case of Rh and Pt combination treatment, both Rh(Amal) and cisplatin were co-administered from 0 – 2 μM. The media was then replaced with fresh media free of Rh or Pt for the remainder of the 72 h experiment. Cells were labeled with BrdU 24 h before analysis, and BrdU incorporation was quantified by antibody assay. Cellular proliferation was expressed as the amount of BrdU incorporated into treated cells compared to that of the untreated controls. Errors were calculated from 5 replicates.

### 3.2.10 ICP-MS Assay for Whole-Cell Rh and Pt Levels

HCT116O cells ($1.0 \times 10^6$) were seeded in 6-well plates containing 3 ml media and allowed 24 h to adhere. The cells were treated with 2 μM of RhPt, Rh(Amal), Pt(Amal), cisplatin, or oxaliplatin and incubated for periods of 1, 3, 6, 12, or 24 h. After the incubation period, the media was decanted and the wells were washed with 4 x 5 ml PBS. The cells were lysed with 1 ml of a 1% sodium dodecyl sulfate (SDS) solution and sonicated using a Qsonica Ultrasonic processor for 20 s at 20% amplitude. A 750 μl aliquot was diluted with 750 μl of a 2% $HNO_3$ (v/v) solution and analyzed for rhodium and platinum content on a Thermo X Series II ICP-MS unit. ICP-MS measurements for platinum content were measured only for the three most abundant naturally occurring isotopes, $^{194}$Pt (33%), $^{195}$Pt (34%), and $^{196}$Pt (25%). The remainder of the cell lysate was analyzed for protein content *via* a bicinchoninic assay (BCA).[24] Rhodium and platinum counts were normalized to protein content to obtain ng [Rh/Pt]/mg [protein], and standard errors were calculated from three replicates.

### 3.2.11 ICP-MS Assay for Nuclear Rh and Pt Levels

HCT116O cells were plated at $1.0 \times 10^7$ cells in 10 ml media and incubated for 24h. The cells were treated with 2 μM of RhPt, Rh(Amal), Pt(Amal), cisplatin, or oxaliplatin and incubated for an additional 24 h. The cells were harvested by trypsinization, washed with cold PBS, and the nuclear fractions were isolated according to established procedures.[16] The nuclear pellets were suspended in 800 μl of Milli-Q water and sonicated on a Qsonica Ultrasonic processor for 20 s at 40% amplitude. A 750 μl aliquot was diluted with 750 μl of a 2% $HNO_3$ (v/v) solution and analyzed for rhodium and platinum content on a Thermo X Series II ICP-MS unit as previously described. The remainder of each sample was used for quantification of nuclear protein content by BCA

analysis. The protein content was then converted to number of nuclei by the conversion factor 3.28 x $10^{-8}$ mg [nuclear protein]/nuclei.[16] Rhodium and platinum counts were then normalized to the number of nuclei, and standard errors were calculated from three replicates.

### 3.2.12 ICP-MS Assay for Mitochondrial Rh and Pt Levels

HCT116O cells were plated at 1.5 x $10^7$ cells/plate and allowed 24 h to adhere. The cells were treated with 2 μM of RhPt, Rh(Amal), Pt(Amal), cisplatin, or oxaliplatin and incubated for an additional 24 h. The cells were harvested by trypsinization, washed with cold PBS, and the mitochondrial fractions were isolated according to established procedures.[16] The mitochondrial pellets were suspended in 800 μl of Milli-Q water and sonicated on a Qsonica Ultrasonic processor for 20 s at 40% amplitude. A 750 μl aliquot was diluted with 750 μl of a 2% $HNO_3$ (v/v) solution and analyzed for rhodium and platinum content on a Thermo X Series II ICP-MS unit as previously described. The remainder of each sample was used for quantification of mitochondrial protein content by BCA analysis. Rhodium and platinum counts were normalized to protein content to obtain ng [Rh/Pt]/mg [mitochondrial protein], and standard errors were calculated from three replicates.

### 3.2.13 MTT Cytotoxicity Assay

The cytotoxic effects of conjugate RhPt, Rh(Amal), Pt(Amal), oxaliplatin, and cisplatin were studied *via* MTT (3-(4,5-dimethylthiazol-2-yl)-2,5-diphenyltetrazolium bromide) assay in the cisplatin-resistant A2780cis and MMR-deficient HCT116O cell lines.[25] Cells were plated in 96-well plates at 50,000 cells/well and incubated with varying concentrations of metal complex (100 nM – 100 μM). For caspase-inhibition

assays, Z-VAD-FMK was added to HCT116O cells to a final concentration of 20 μM. For poly-ADP ribose polymerase (PARP) assays, the inhibitor 3,4-dihydro-5[4-(1-piperindinyl)butoxy]-1(2*H*)-isoquinoline (DPQ) was added to HCT116O cells to a final concentration of either 25 or 50 μM. Cells were incubated under humidified atmosphere for 72 h and labeled with MTT for an additional 4 h at 37 °C, 5% $CO_2$. The ensuing formazan crystals were dissolved with a lysis buffer (10% SDS in 10 mM HCl) according to the manufacturer's instructions. MTT reduction to formazan was quantified by electronic absorption at 570 nm (background: 690 nm), and percent viability was expressed as the amount of formazan in treated cells compared to that of the untreated controls. The data were plotted in OriginPro 8.5 and fit to a sigmoidal curve. Errors were calculated from 5 replicates.

### 3.2.14 Preparation of Cell Extracts for *In Vitro* DNA Replication Assay

Cell extracts were prepared according to published protocols, with slight modifications.[26] HCT116O cells were plated at 1.0 x $10^7$ cells/plate and allowed 24h to adhere. Cells were treated with varying concentrations of platinum and allowed to grow for an additional 6h; a plate of untreated cells was incubated alongside platinum-treated cells as a control. Cells were harvested by trypsinization, washed with cold PBS, and resuspended in 1 ml hypotonic cell extraction buffer (20 mM HEPES (pH 7.5), 5 mM KCl, 1.5 mM $MgCl_2$, 1 mM DTT, protease inhibitors). Cell suspensions were incubated on ice for 10 min before lysis *via* 7 passages through a 25-gauge needle in a 1-ml syringe. Cell lysates were incubated on ice for 30 min and centrifuged at 10,000 x *g* at 4 °C for 10 min. The clarified lysate was collected as the supernatant, aliquoted, and stored at -80 °C. Protein concentration was determined *via* BCA assay.

### 3.2.15 *In Vitro* SV40 DNA Replication Assay

The cell-free simian virus 40 (SV40) DNA replication assay was carried out according to published protocols, with minor modifications.[26,27] Briefly, 25 μl replication reactions were prepared, each containing 30 mM HEPES (pH 7.5); 7 mM $MgCl_2$; 0.5 mM DTT; 4 mM ATP; 100 μM each of dATP, dGTP, dCTP, and dTTP; 50 μM each of CTP, GTP, and UTP; 40 mM phosphocreatine; 0.625 units creatine phosphokinase; 1 μCi [α-$^{32}$P]dCTP; 50 ng SV40 origin-containing pUC HSO plasmid DNA; 1 μg SV40 large T antigen (T-Ag); and 40 μg HeLa cell extract. Sterile water was added to bring the reaction to a final volume of 25 μl, and the reaction was incubated at 37 °C for 4 h. The reaction was quenched *via* addition of an equal volume of stop solution (30 mM EDTA, 0.5% SDS, 200 μg/ml proteinase K (New England BioLabs). After incubation for 30 min at 37 °C, replication products were purified by ethanol precipitation (500 μl EtOH, 50 μl 7.5M $NH_4OAc$, 50 μl yeast RNA co-precipitant) and electrophoresed on a 1% agarose gel. The amounts of DNA in each band were analyzed by autoradiography and quantitated by phosphorimagery (ImageQuant).

## 3.3 Results

### 3.3.1 Complexes Synthesized

We report the synthesis and characterization of a bimetallic conjugate (RhPt, **Figure 3.1**), in which an oxaliplatin derivative is tethered to a rhodium metalloinsertor through an aminomalonate leaving group ligand. The conjugate was constructed *via* a linear synthesis, in which the trisheteoleptic rhodium (III) scaffold (Synthesis shown in **Scheme 3.1**) was first functionalized with diethyl aminomalonate, followed by saponification of the diester and subsequent complexation to the platinum center

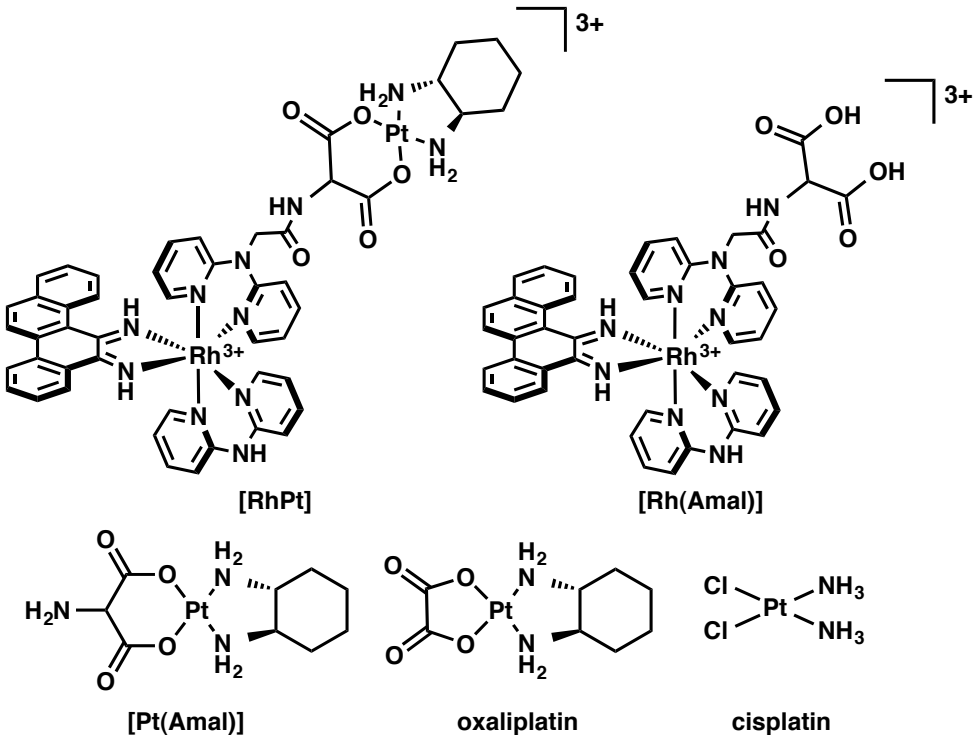


**Figure 3.1** Chemical structures of complexes studied. RhPt is a bifunctional conjugate comprised of a trisheteroleptic rhodium metalloinsertor, which recognizes DNA mismatches, tethered to a *cis*-platinum (II) anticancer agent derived from oxaliplatin, which forms covalent adducts with DNA at guanine residues, through the platinum leaving group ligand. Rh(Amal) is the product resulting from the eventual hydrolysis of the platinum subunit of RhPt. Pt(Amal) is the platinum subunit of RhPt. Oxaliplatin and cisplatin are FDA-approved chemotherapeutic agents that form cytotoxic covalent crosslinks with DNA.

(**Scheme 3.2**). The platinum moiety employs the same (1*R*,2*R*)-1,2-diaminocyclohexane non-leaving group ligand as oxaliplatin, and therefore is expected to form the same DNA adducts.[28] The rhodium subunit contains a sterically expansive 5,6-chrysene diimine ligand (chrysi), which is responsible for the recognition of DNA mismatches.[11,12] The aminomalonate linker is tethered to one of the non-inserting ancillary ligands, which allows the conjugate to remain intact temporarily, but ultimately enables the release of platinum, *via* hydrolysis, for DNA binding. The remaining complexes included in this work are also depicted in **Figure 3.1**. The rhodium hydrolysis product, Rh(Amal) (Compound ***2*** in **Scheme 3.2**), was included as a control to ensure that the biological activity of RhPt is the result of the intact conjugate and not premature hydrolysis of the subunits. The unconjugated platinum complex, Pt(Amal), was also included to account for the effects of the aminomalonate ligand on activity. The synthesis of Pt(Amal) is shown in **Scheme 3.3** The FDA-approved chemotherapeutics oxaliplatin and cisplatin were also included for comparison.

### 3.3.2 DNA Binding Studies

#### 3.3.2.1 Binding Affinity of Rhodium at a CC Mismatch

*In vitro* DNA binding studies were performed with RhPt and radiolabeled duplex DNA containing a CC mismatch (**Figure 3.2**) with the sequence 5*'-TTAGGATCATCCATATA-3' (underline denotes the mismatch, asterisk denotes the radiolabel). The RhPt conjugate was bound with mismatched and well-matched duplex DNA (of the same sequence, but annealed to a fully matched complement) at varying concentrations and irradiated (340-440 nm) for 15 min. Samples were then incubated at 37 °C for 10 min to promote the formation of platinum adducts and subsequently

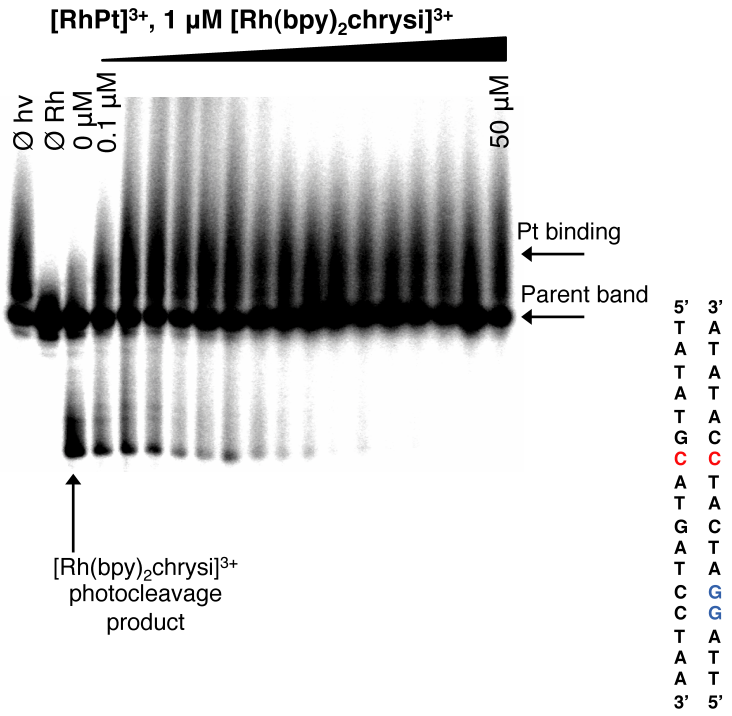


**Figure 3.2** Competition titration of increasing concentrations of RhPt (0-50 µM) with 1 µM *rac*-[Rh(bpy)$_2$chrysi]$^{3+}$ on 1 µM 5'-[$^{32}$P] labeled 17mer duplex DNA with a CC mismatch (denoted in red) and a d(GpG) site (denoted in blue). Samples were irradiated (340-440 nm) for 15 min and electrophoresed on a 20% denaturing polyacrylamide gel. Controls without irradiation (Øhν), and without Rh (ØRh) were included. RhPt inhibits photocleavage by [Rh(bpy)$_2$chrysi]$^{3+}$ at the mismatched site. The site of photocleavage by [Rh(bpy)$_2$chrysi]$^{3+}$ at the mismatch is indicated by an arrow at bands located below the unmodified parent band. Bands of reduced electrophoretic mobility, located above the unmodified parent DNA, are indicative of covalent binding by the platinum subunit.

electrophoresed on a denaturing PAGE gel. As RhPt does not cleave DNA upon irradiation, a competition titration was carried out using *rac*-$[Rh(bpy)_2chrysi]^{3+}$, which does photocleave DNA at the site of a mismatch.[10] RhPt inhibits photocleavage by *rac*-$[Rh(bpy)_2chrysi]^{3+}$ at the mismatched site in a dose-dependent manner (**Figure 3.2**); this indicates that RhPt binds specifically to the mismatch *via* metalloinsertion. The amount of photocleaved DNA was quantified and plotted against the logarithmic concentration of RhPt (log[RhPt]), and the $K_B$ value of RhPt was calculated by solving simultaneous equilibria at the inflection point of the titration curve (**Figure 3.3**). The binding affinity of RhPt for a CC mismatch was determined to be 1.1 x $10^7$ $M^{-1}$, comparable to that of monomeric metalloinsertors.[14,16,17]

#### 3.3.2.2 Platinum Binding to DNA

DNA binding by the conjugate also involves the formation of covalent adducts. As the platinum subunit dissociates from the conjugate *via* hydrolysis, it can covalently crosslink with DNA. Platination of the DNA is indicated by the appearance of bands with reduced electrophoretic mobility, located above the unmodified parent bands in the autoradiogram (**Figure 3.2**). The amount of platinated DNA (expressed as a fraction of the total DNA) was plotted against log[RhPt] and fit to a sigmoidal curve (**Figure 3.4**). At higher concentrations, platination diverges from the curve, but does not exceed a 1:1 ratio of Pt:DNA. No difference in platination levels was observed in DNA binding experiments with well-matched DNA.

#### 3.3.2.3 Dimethyl Sulfate Footprinting of Pt-DNA Crosslinks

Platinum binding to DNA was further characterized by dimethyl sulfate (DMS) footprinting. DMS methylates the *N*7 position of guanine, resulting in cleavage at those

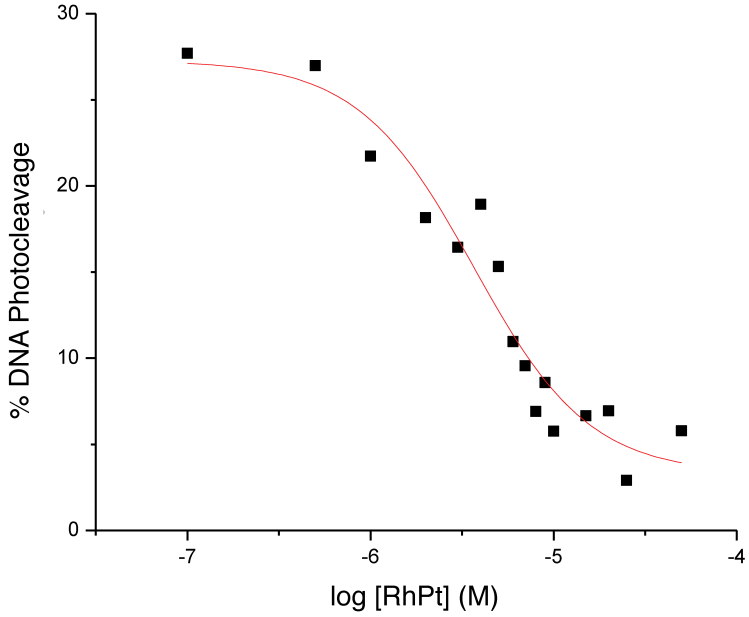


**Figure 3.3** Representative sigmoidal curve (Boltzmann fit) of photocleavage competition titrations of RhPt for binding constant determination at the CC mismatch. $K_B$ was calculated by solving simultaneous equilibria at the inflection point of the curve. Experiments were conducted in buffer (50 mM NaCl, 10 mM $NaP_i$, pH 7.1) using 1 μM duplex DNA and 1 μM rac-$[Rh(bpy)_2chrysi]^{3+,}$ with 0-50 μM RhPt competitor complex. The binding constant was determined from three independent experiments.

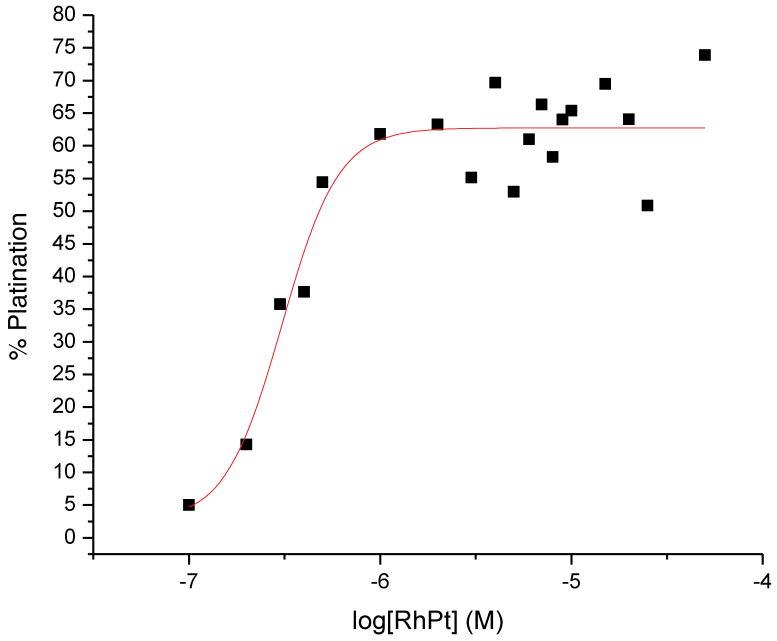


**Figure 3.4** Representative sigmoidal curve fit of DNA platination by the platinum subunit of RhPt, from 0-50 μM. RhPt was incubated with duplex DNA containing a CC mismatch and a d(GpG) site at 37 °C for 10 min to promote the formation of covalent Pt-DNA adducts. Samples were electrophoresed on a 20% denaturing PAGE gel. The amount of platinated DNA is expressed as a fraction of the total DNA in each sample.

sites upon treatment with piperidine.[22] Duplex DNA (1 μM) containing a single CC mismatch (see **Section 3.3.2.1** for sequence) was radiolabeled at the 5'-end with [$^{32}$P] and incubated with either oxaliplatin or RhPt for 90 min at 37 °C to promote the formation of Pt-DNA adducts. The DNA was then subjected to treatment with DMS, followed by piperidine cleavage. Free guanine residues – i.e., those not coordinated to platinum – are expected to be methylated at the N7 position by DMS and therefore susceptible to piperidine cleavage. At a 1:1 molar ratio of DNA and RhPt (**Figure 3.5**), the guanine residues on the labeled strand are protected from cleavage, signifying the formation of platinum 1,2-intrastrand adducts at the *N*7 positions of the d(GpG) site, as is the case for oxaliplatin.

Adenine methylation is also observed with DMS treatment (visible in the autoradiogram at high gain), but there is no evidence of platinum binding at these sites. At 50 μM RhPt (50 fold excess), only one guanine is protected, possibly due to distortions to the DNA that impede the formation of 1,2-d(GpG) adducts.

### 3.3.3 Quantitation of Inhibition of Cellular Proliferation Using an Enzyme-Linked Immunosorbent Assay (ELISA)

An ELISA for DNA synthesis was used to quantify the effects of RhPt and the corresponding control complexes on the proliferation of HCT116N (MMR-proficient) cells and HCT116O (MMR-deficient) cells.[29] Cells were treated with 0 – 2 μM of each complex (including a control where Rh and Pt complexes were added together but as separate subunits, at equal concentrations) and incubated for 24h. Thymidine analogue BrdU, which is incorporated in place of thymidine during DNA synthesis, was added to cells 24h prior to analysis. The extent of cellular proliferation was determined *via*

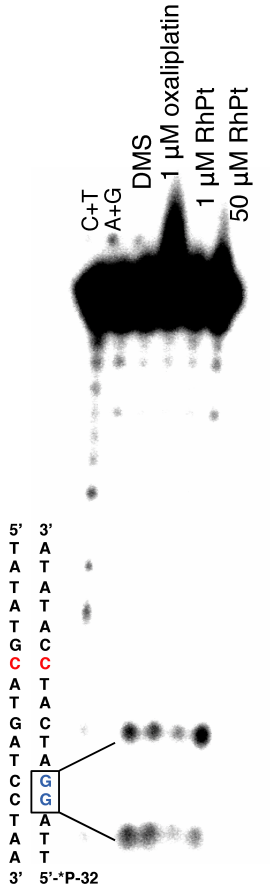


**Figure 3.5** Dimethyl sulfate (DMS) footprinting of 5'-end radiolabeled duplex DNA containing a CC mismatch (denoted in red) and a d(GpG) site (denoted in blue, boxed). Samples were incubated with platinum and treated with 10% DMS, followed by piperidine cleavage. Samples were electrophoresed on a 20% denaturing PAGE gel. Lanes (left to right): Maxam Gilbert sequencing (C+T; A+G); DMS alone; oxaliplatin (1 μM); RhPt (1 μM); RhPt (50 μM). Bands of high electrophoretic mobility indicate cleavage at guanine residues; covalent binding of platinum to guanine inhibits cleavage. Both oxaliplatin and RhPt form covalent 1,2-intrastrand Pt-DNA adducts at the *N*7 position of guanine.

quantification of the amount of BrdU incorporated into treated cells normalized to that of untreated cells, as determined by antibody detection.[23]

The results of the ELISA for RhPt compared to FDA-approved therapeutics oxaliplatin and cisplatin in the two cell lines are shown in **Figure 3.6**. No cell-selectivity was observed for RhPt; the complex inhibits growth in both HCT116N and HCT116O cell lines equally. Additionally oxaliplatin also does not display any preferential targeting of either cell line, but cisplatin exhibits a slight preference for the MMR-proficient HCT116N cell line, as has been observed in previous studies;[30] overall, however, cisplatin exhibits low potency at the concentration range explored in this work. RhPt exhibits antiproliferative activity similar to that of oxaliplatin and considerably outperforms cisplatin, inhibiting cell proliferation at concentrations as low as 500 nM after 24h incubation. All complexes were probed at 0-2 μM in both cell lines as shown in **Figure 3.6**, but neither Pt(Amal) nor Rh(Amal) shows any preferential targeting of either cell line – Pt(Amal) targets both cell lines equally and Rh(Amal) displays little antiproliferative effect at the concentrations indicated (data not shown).

The inhibitory effects of all complexes on HCT116O cells at 2 μM after 24h incubation are shown in **Figure 3.7**. At 2 μM, RhPt inhibits cellular proliferation by 79 ± 1%, compared to 75 ± 3% for oxaliplatin. Interestingly, RhPt exhibits increased activity compared to either of its monomeric subunits alone: at 2 μM, Pt(Amal) inhibits cell proliferation by 65 ± 2%, while Rh(Amal) inhibition is only 17 ± 4%. At 2 μM cisplatin treatment, to which HCT116O cells are known to exhibit resistance, DNA synthesis is stalled by only 27 ± 3%, and co-treatment of cisplatin with the rhodium subunit confers little synergistic effect.

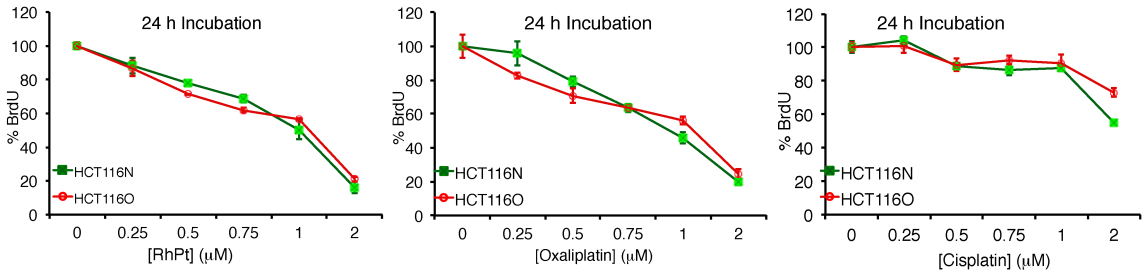


**Figure 3.6** Inhibitory effects of RhPt (left), oxaliplatin (center), and cisplatin (right) on cellular proliferation. DNA synthesis is shown as a function of percent BrdU incorporation normalized to that of untreated cells. MMR-proficient HCT116N (green) and MMR-deficient HCT116O (red) cells were plated in 96-well plates and allowed 24 h to adhere. Cells were then treated with 0-2 μM of the indicated metal complex for 24 h, after which the medium was removed and replaced with fresh, drug-free medium for the remainder of the 72 h period. BrdU was added to the medium 24 h prior to ELISA analysis. Standard error bars were calculated from 5 replicates.

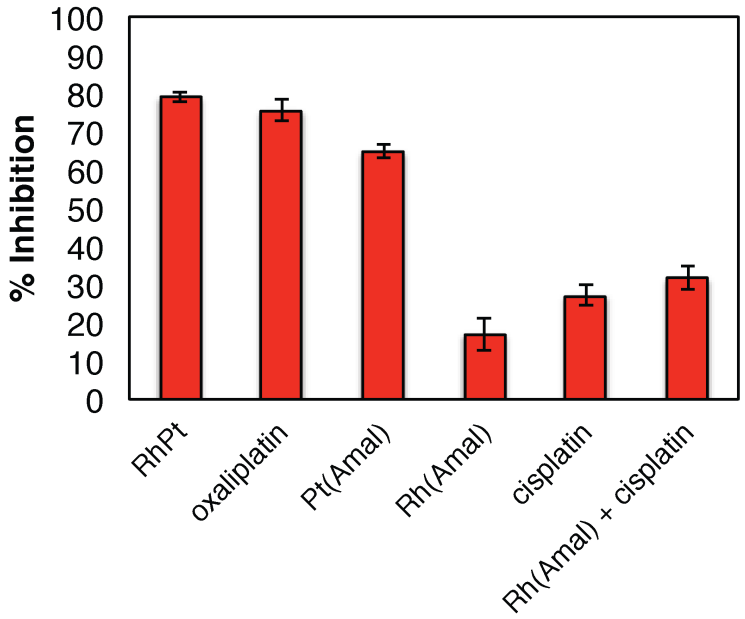


**Figure 3.7** Inhibitory effects of all complexes on cellular proliferation in HCT116O cells after 24 h treatment with 2 μM of each complex. For combination treatment, cells were treated with 2 μM each of cisplatin and Rh(Amal). Treatment of cells with the unconjugated Rh(Amal) in combination with the relatively non-potent cisplatin compound has no significant effect on overall inhibition of growth. Percent inhibition is expressed as the normalized percent BrdU incorporation subtracted from 100% (i.e., untreated cells, normalized). Standard errors were calculated from 5 replicates.

### 3.3.4 Cell-Free SV40 DNA Replication Assay

The inhibitory properties of RhPt were also explored in an *in vitro*, cell-free DNA replication assay, to corroborate the results of the ELISA. Here, the soluble extracts of eukaryotic cells could be tested for their ability to carry out replication on exogeneous viral DNA in the presence of *cis*-platinum. Simian virus 40 (SV40) is a well-characterized model system for the examination of DNA replication *in vitro*.[26] Requiring only the SV40 large tumor antigen (T-Ag), dNTPs, and the SV40 origin of replication, DNA synthesis can be carried out using the native proteins supplied by the eukaryotic cell extract.[26,27]

To each *in vitro* replication reaction was added 40 μg soluble HeLa (procured in kit form) or 25 μg HCT116O (isolated according to the procedure described in **Section 3.2.14**) cell extract, and either oxaliplatin to a final concentration of 0 or 2 μM, or RhPt to a final concentration of 0, 2, 10, or 20 μM. Replication of pUC HSO plasmid DNA containing the SV40 origin was carried out at 37 °C for 4h in the presence of radiolabeled [α-$^{32}$P]dCTP. A mock reaction containing HSO plasmid DNA lacking the SV40 origin was included as a negative control. Replication products were isolated, separated by non-denaturing agarose gel electrophoresis, and identified by autoradiography.

In the initial studies carried out with HCT116O cell extract, no appreciable replication could be observed, even in the absence of platinum (**Figure 3.8**). It is possible that the HCT116O cells require a different cell extraction protocol in order to obtain active cell lysate. It is also possible that HCT116O cell extract cannot support *in vitro* replication of viral DNA. As the positive control using the commercially provided HeLa

cell extract appeared to work (**Figure 3.8**, Lane 1), the remainder of the experiments were carried out using HeLa lysate.

The effects of platinum treatment on SV40 replication in HeLa extract are shown in **Figure 3.9**. As expected based on the results in the ELISA, both oxaliplatin and RhPt significantly inhibit replication of SV40 origin-containing DNA. RhPt exhibits a dose-depenent response. However, RhPt and oxaliplatin treatment have differing effects on the replication products produced. Treatment with 2 μM oxaliplatin results in a marked decrease in the formation of all replication products: circular supercoiled DNA (Form I), circular nicked DNA (Form II), and linear DNA (Form III). In contrast, treatment with 2 μM RhPt yields a slight increase in Form I product compared to the untreated control, but a significant decrease in Form II and Form III DNA is observed. It is possible that the cellular processing of oxaliplatin adducts differs somewhat from that of RhPt; nevertheless, it is clear that these results support those observed in the ELISA in that RhPt stalls replication and DNA synthesis in a cellular environment.

### 3.3.5 MTT Cytotoxicity

The cytotoxic effects of all complexes were probed *via* MTT assay. Metabolically active cells are capable of reducing the yellow tetrazole (3-(4,5-dimethylthiazol-2-yl)-2,5-diphenyltetrazolium bromide (MTT) to purple formazan crystals, which can be dissolved in acidified SDS to obtain a characteristic absorbance at 570 nm. Quantification of formazan by electronic absorption indicates the amount of metabolically active cells in each sample. MMR-deficient human colorectal carcinoma HCT116O cells and cisplatin-resistant A2780cis human ovarian cancer cells were treated with a broad concentration range of metal complex (100 nM – 100 μM) and incubated for 72h. The percent viability

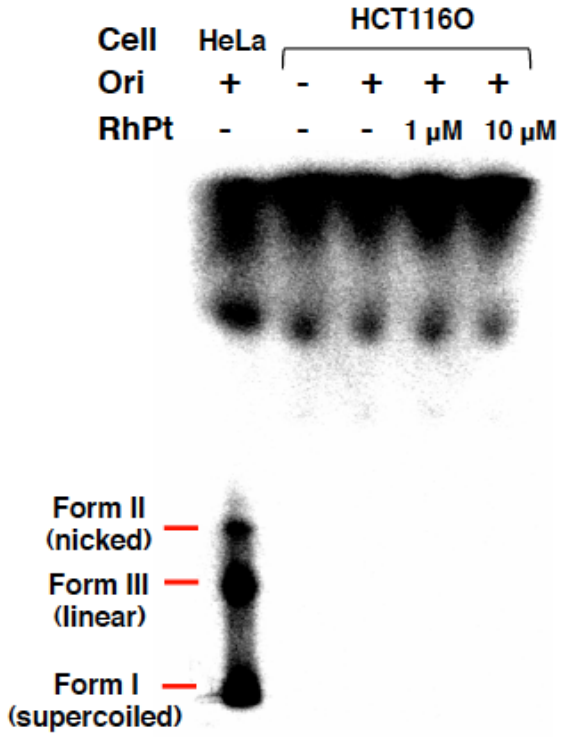


**Figure 3.8** Cell-free *in vitro* SV40 replication assay. HCT116O cells were plated at 1 x $10^7$ cells and allowed 24 h to adhere. Cells were then treated with 0, 1, or 10 μM RhPt for 6 h, harvested, and soluble cell lysates were isolated. Cell lysates were incubated with SV40-origin containing plasmid DNA in the presence of [α-$^{32}$P]dCTP at 37 °C for 4 h. Untreated HeLa cell extract was included as a positive control, and untreated HCT116O cell extract in the presence of plasmid DNA lacking the SV40 origin ("Ori –") was included as a negative control. No replication is observed for any of the HCT116O cell extracts.

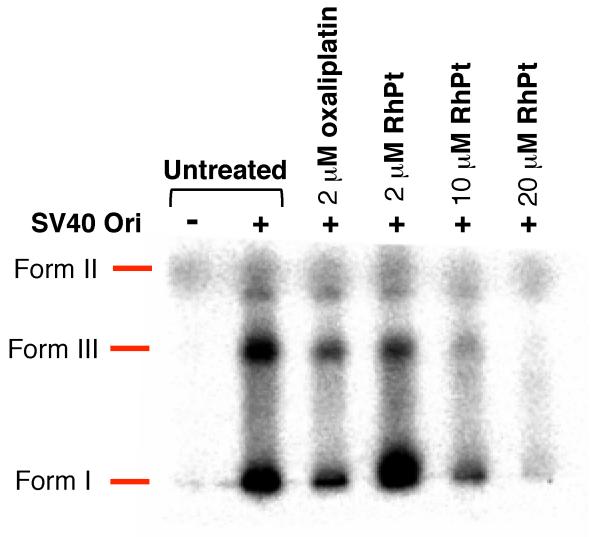


**Figure 3.9** Cell-free *in vitro* SV40 replication assay. Hela cell extract was treated with either oxaliplatin (2 μM) or RhPt (2, 10, or 20 μM) and allowed to replicate plasmid DNA containing the SV40 origin in the presence of [α-$^{32}$P]dCTP at 37 °C for 4 h. A reaction was carried out on plasmid DNA lacking the SV40 origin as a negative control ("Ori –"). A positive control containing untreated HeLa extract was also included. Treatment with 2 μM oxaliplatin decreases the levels of all replication products – Form I (supercoiled), Form II (circular nicked), and Form III (linear). Treatment with RhPt confers a dose-dependent effect on SV40 replication. Initially, the presence of RhPt results in a decrease of Form II and Form III DNA, primarily. At higher concentrations (10 μM and above), a decrease in all replication products is observed.

is defined as the amount of formazan in cells treated with rhodium and/or platinum normalized to that of untreated cells. The dose-response curves for HCT116O and A2780cis cells are shown in **Figure 3.10** and **Figure 3.11**, respectively. For HCT116O cells, RhPt (shown in black in **Figure 3.10**) is the most potent of all complexes studied. The A2780cis cell line exhibits a similar sensitivity to RhPt (shown in black in **Figure 3.11**) as the HCT116O line; however, oxaliplatin and Pt(Amal) are significantly more active in A2780cis cells.

$LC_{50}$ values, defined as the concentration at which 50% of the cells are viable after 72h treatment with metal complex, were also determined for all of the complexes, which are summarized in **Table 3.1**. With an $LC_{50}$ value of 9.01 μM, RhPt exhibits a 3-fold increase in cytotoxicity over both oxaliplatin and cisplatin in the HCT116O cell line, and is also significantly more potent than either of its unconjugated components. This is in contrast to its activity in the A2780cis cells: while RhPt exhibits similar potency in this cell line ($LC_{50}$ = 8.9 μM), its monomeric platinum counterpart Pt(Amal) is significantly more potent.

### 3.3.6 ICP-MS Assay for Whole-Cell Rhodium and Platinum Levels

As RhPt displays high cytotoxicity but no preferential targeting of MMR-deficient cells, we next explored whether its cellular uptake properties explained its enhanced potency. HCT116O cells were treated with 2 μM metal complex for periods of 1, 3, 6, 12, or 24h. The cell lysates were then analyzed for rhodium and/or platinum content by inductively coupled plasma mass spectrometry (ICP-MS) and normalized to protein content as determined by BCA assay (See **Section 3.2.10**). The cellular uptake of platinum for RhPt, oxaliplatin, cisplatin, and Pt(Amal) is depicted in Figure **3.12a**.

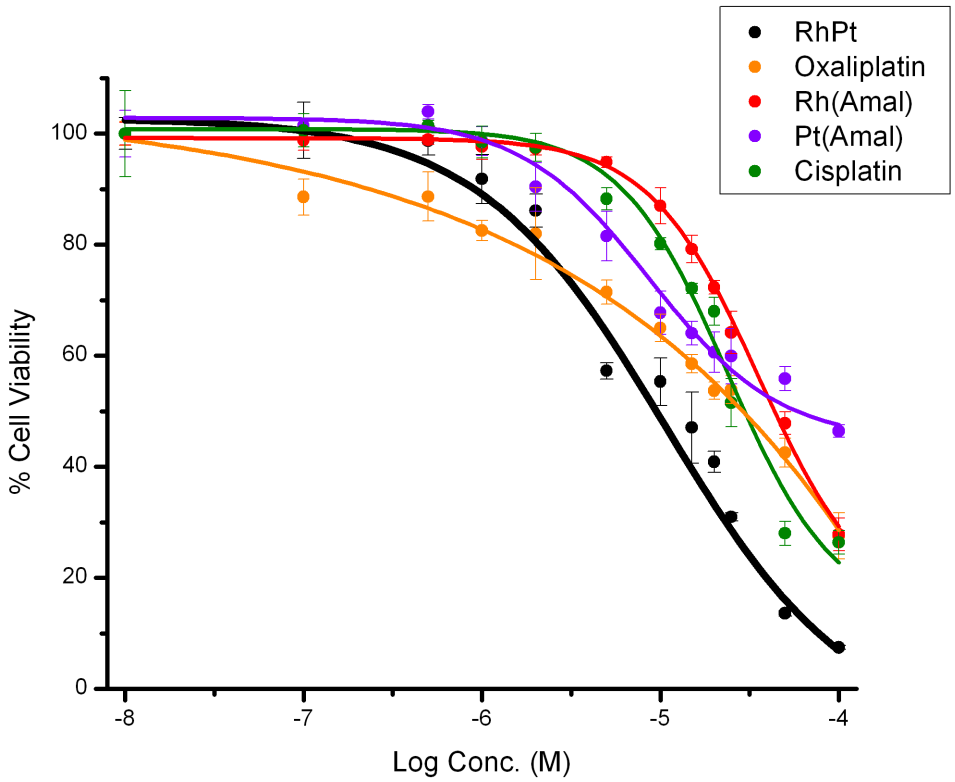


**Figure 3.10** Dose-response cytotoxicity curves of HCT116O cells treated with RhPt (black), oxaliplatin (orange), Rh(Amal) (red), Pt(Amal) (purple), and cisplatin (green). Cells were treated with 0-100 μM of each metal complex and incubated for 72 h. After the incubation period, cells were treated with the MTT reagent for 4 h, and the resulting formazan crystals were solubilized with acidified SDS. Percent cell viability is defined as the percentage of formazan normalized to that of untreated cells. Data were fit to a sigmoidal curve, and $LC_{50}$ values were obtained (See **Table 3.1**). Standard errors were calculated from 5 replicates.

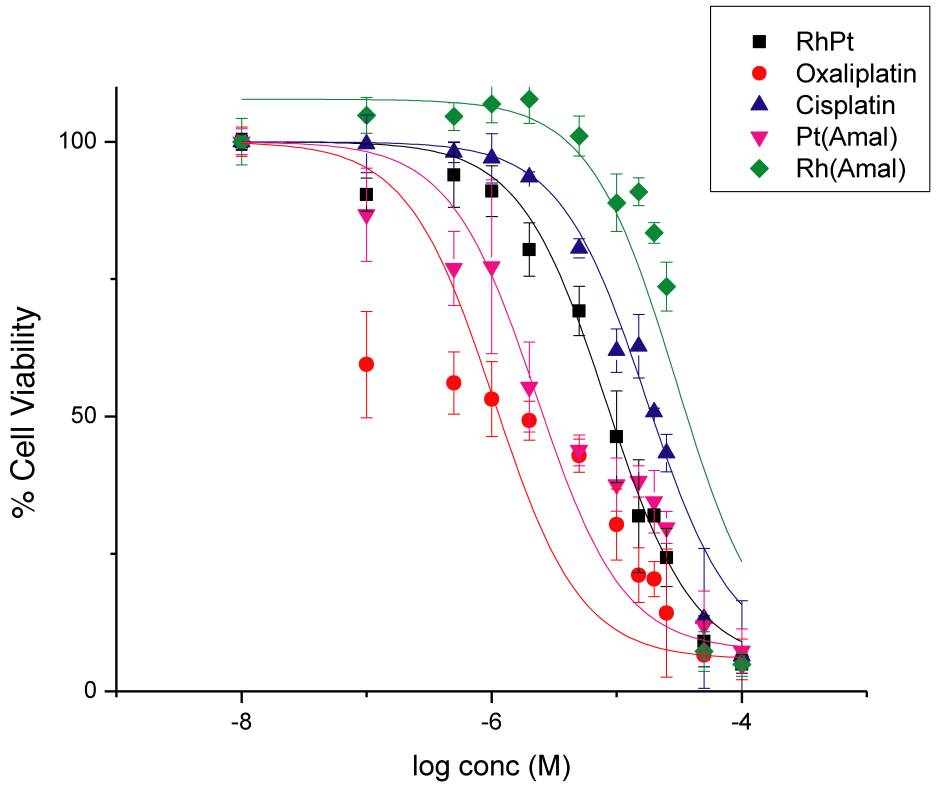


**Figure 3.11** Dose-response cytotoxicity curves of cisplatin-resistant A2780cis cells treated with RhPt (black), oxaliplatin (red), Rh(Amal) (green), Pt(Amal) (fuschia), and cisplatin (blue). Cells were treated with 0-100 μM of each metal complex and incubated for 72 h. After the incubation period, cells were treated with the MTT reagent for 4 h, and the resulting formazan crystals were solubilized with acidified SDS. Percent cell viability is defined as the percentage of formazan normalized to that of untreated cells. Data were fit to a sigmoidal curve, and $LC_{50}$ values were obtained (See **Table 3.1**). Standard errors were calculated from 5 replicates.

**Table 3.1** $LC_{50}$ Values[a] of Metal Complexes in HCT116O and A2780cis Cells

| **Complex** | **$LC_{50}$ HCT116O** | **$LC_{50}$ A2780cis** |
|---|---|---|
| RhPt | 9.01 μM | 8.9 μM |
| Oxaliplatin | 27.5 μM | 1.15 μM |
| Cisplatin | 29.5 μM | 18.7 μM |
| Pt(Amal) | 43.3 μM | 2.66 μM |
| Rh(Amal) | 57.2 μM | 35.9 μM |

[a] $LC_{50}$ refers to the concentration at which 50% of the cells are viable after 72 h, as determined by MTT assay. Cells were plated in 96-well plates at densities of 5 x $10^4$ cells/well and treated with varying concentrations of the indicated metal complex. After the 72 h period, cells were treated with MTT for an additional 4 h. The resulting formazan crystals were solubilized with a solution of 10% SDS and 10 mM HCl, and absorbances were recorded at 570 nm. $LC_{50}$ values were calculated from the titration curves of three independent experiments

Across all time points (except for 24 h), the platinum content of RhPt (blue bars) far exceeds that of the monomeric platinum complexes studied. The mechanism of platinum uptake for RhPt also seems to differ from that of the other platinum complexes. Cellular accumulation of RhPt is relatively high at earlier time points, but steadily decreases after 6h, possibly due to an efflux mechanism. By contrast, oxaliplatin (orange bars) displays a relatively high initial uptake at 1 h, followed by a decrease in platinum content at 3 h, with little change at later time points. The cellular concentration of cisplatin (green bars) is comparatively quite low, and remains largely unchanged over the 24 h period. Pt(Amal) (purple bars), the monomeric platinum counterpart of RhPt, exhibits uptake similar to that of cisplatin, with only slight increases in platinum content after 1 h.

The cellular uptake of rhodium is shown adjacently in **Figure 3.12b**. For RhPt (gray bars), the cellular rhodium content exceeds that of platinum, suggesting that the conjugate hydrolyzes at some point. However, comparison to the cellular uptake of the synthesized hydrolysis product, Rh(Amal) (red bars), shows that the rhodium uptake is significantly higher – nearly an order of magnitude at some time points – in cells treated with RhPt. Furthermore, the pattern of cellular uptake over time differs for the two complexes, with RhPt displaying high rhodium uptake at early timepoints, followed by a gradual decrease at later time points – highly similar to the uptake patterns of the platinum subunit. The cellular rhodium content of Rh(Amal), in contrast remains largely unchanged over the 24 h period. Therefore, the divergence in rhodium vs. platinum accumulation for RhPt is unlikely due to significant conjugate hydrolysis occurring prior to being taken up into the cell.

### 3.3.7 ICP-MS Assay for Nuclear Rhodium and Platinum Levels

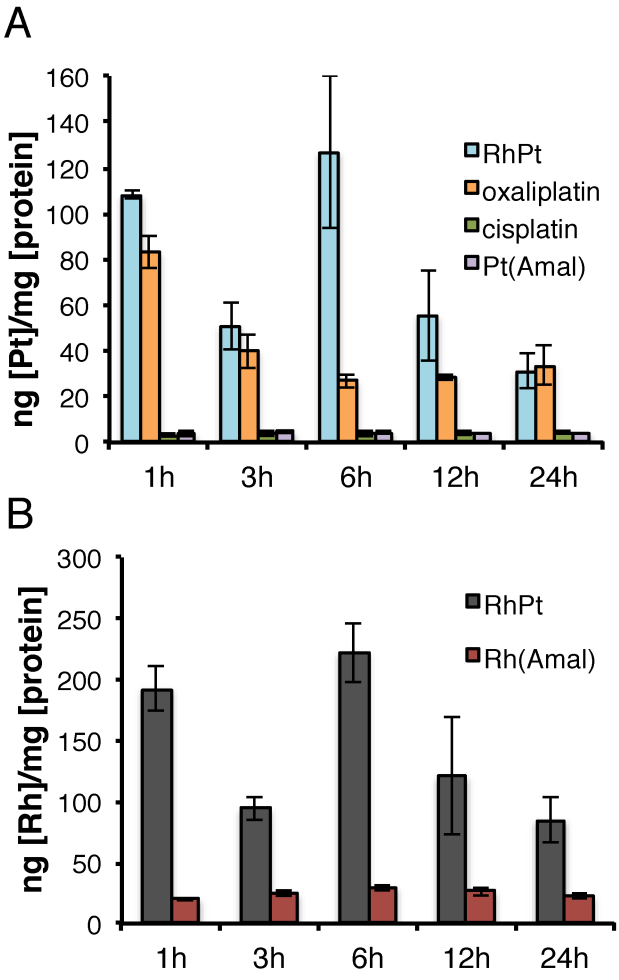


**Figure 3.12** Cellular accumulation of metal complexes in HCT116O cells. Adherent cells (1 x $10^6$) were treated with 2 μM complex for the durations indicated. Cells were analysed for rhodium and platinum content by ICP-MS, and normalized to cellular protein content as determined by BCA assay. (A) Whole-cell platinum uptake of RhPt (blue), oxaliplatin (orange), cisplatin (green), and Pt(Amal) (purple). (B) Whole-cell rhodium uptake of RhPt (gray) compared to hydrolysis product Rh(Amal) (red).

The nuclear uptake of all complexes were determined using ICP-MS. HCT116O cells were treated with 2 μM metal complex for 24 h, and the nuclei were isolated as described above. Rhodium and platinum levels were measured via ICP-MS and normalized to the number of nuclei. The nuclear rhodium and platinum levels for RhPt are shown in **Figure 3.13a** (left axis), expressed as ng [metal]/nuclei. Rhodium uptake is depicted in gray, and platinum uptake is shown in blue. The nuclear concentrations of the two metals are similar, indicating that nuclear uptake of the intact conjugate may be occurring. The nuclear rhodium uptake was compared between RhPt and Rh(Amal) and is shown in **Figure 3.13b** (left axis). Significantly, the nuclear rhodium uptake of RhPt exceeds that of Rh(Amal) by nearly an order of magnitude, which further supports the notion that RhPt is taken up into the nucleus as an intact conjugate, rather than hydrolyzing beforehand.

Figure **3.13c** (left axis) shows nuclear platinum levels of the remaining complexes compared to RhPt, expressed as ng [Pt]/nuclei. Overall, there is little variation in the nuclear uptake of platinum. As a result, it is unlikely that the enhanced potency of RhPt can be attributed to nuclear localization alone.

The levels of nuclear rhodium and platinum for all complexes were converted to molar concentrations by approximating the nucleus of an HCT116 cell as a sphere with radius 4 μm.[31] The values are summarized in **Table 3.2**. Notably, RhPt localizes to the nucleus in concentrations sufficient for rhodium mismatch binding (given its *in vitro* binding affinity) yet below nonspecific DNA binding levels.[16]

### 3.3.8 ICP-MS Assay for Mitochondrial Rhodium and Platinum Levels

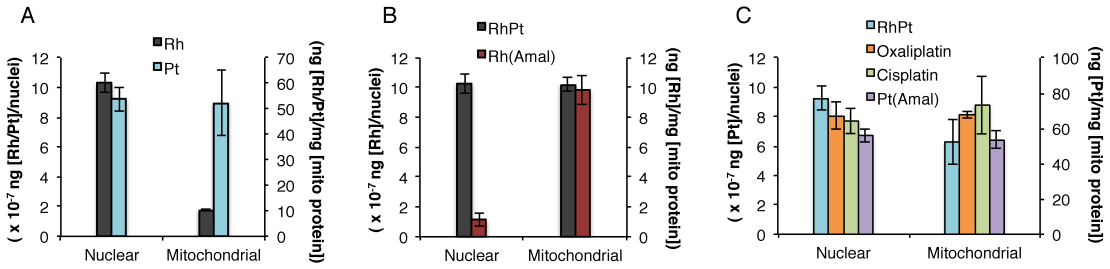


**Figure 3.13** Subcellular localization of metal complexes. HCT116O cells were incubated with 2 μM metal complex for 24h, and the appropriate organelle isolation procedures were performed. Metal content was analyzed by ICP-MS and normalized to protein content as determined by BCA assay. Nuclear metal content is expressed as ng[Metal]/nuclei, and mitochondrial metal content is expressed as ng[M]/mg [mitochondrial protein]. (A) Nuclear (left axis) and mitochondrial (right axis) uptake of RhPt. The uptake of rhodium is shown in gray, and platinum is shown in blue. (B) Nuclear (left axis) and mitochondrial (right axis) uptake of rhodium for RhPt (gray) and hydrolysis product Rh(Amal) (red). (C) Nuclear (left axis) and mitochondrial (right axis) uptake of platinum for RhPt (blue), oxaliplatin (orange), cisplatin (green), and Pt(Amal) (purple).

**Table 3.2 Subcellular Distribution of Metal Complexes in HCT116O Cells***

| Complex | Nuclear[a] | Mitochondrial[b] |
|---|---|---|
| RhPt | 18 ± 2 μM Pt<br>37 ± 2 μM Rh | 52 ± 13 Pt<br>10 ± 0.4 Rh |
| Rh(Amal) | 4 ± 1 μM | 9.8 ± 0.9 |
| Pt(Amal) | 13 ± 1 μM | 54 ± 5 |
| Oxaliplatin | 15 ± 2 μM | 68 ± 2 |
| Cisplatin | 14 ± 2 μM | 73 ± 17 |

*Nuclear versus mitochondrial metal uptake are normalized differently, mitigating their comparison. [a] Nuclear concentrations were obtained by dividing metal content by the volume of the nucleus, estimated as a sphere with radius 4 μm.[31] Errors were calculated from three replicates. [b] Mitochondrial metal content is normalized to mitochondrial protein using by BCA analysis, and is expressed as (ng [metal]/mg [mito protein]).

The complexes were also analyzed for mitochondrial localization. HCT116O cells were treated with 2 μM metal for 24 h, and mitochondria were isolated as described above. Rhodium and platinum counts were determined by ICP-MS and normalized to mitochondrial protein content, as determined by BCA assay. The mitochondrial localization of rhodium and platinum for all complexes are shown in **Figure 3.13** and summarized in **Table 3.2**. The mitochondrial localization of rhodium and platinum for RhPt is depicted in **Figure 3.13a** (right axis). Unlike the nuclear metal content, the mitochondrial rhodium and platinum levels differ substantially, with mitochondrial platinum uptake ~5 fold greater than that of rhodium. Again, comparison of RhPt with its hydrolysis counterpart, Rh(Amal), offers further insight into the biological behavior of the conjugate. Figure **3.13b** (right axis) displays the mitochondrial rhodium content for the two complexes, and they are nearly identical, with 10 ± 0.4 ng [Rh]/mg [mitochondrial protein] for RhPt, and 9.8 ± 0.9 ng [Rh]/mg [mitochondrial protein] for Rh(Amal). The highly similar rhodium content of RhPt and Rh(Amal) further suggests that the conjugate has hydrolyzed, and that the rhodium and platinum subunits enter the mitochondria as separate entities.

Mitochondrial platinum content is shown in **Figure 3.13c** (right axis). Mitochondrial localization does not appear to correlate with cytotoxicity, cellular uptake, or nuclear localization, and in fact the mitochondrial platinum content is quite similar across all complexes. Overall, it does not appear that the subcellular localization of platinum plays a significant role in altering the biological behavior of the complexes in this work.

### 3.3.9 Caspase and PARP Inhibition Assays

To further understand the biological activity of RhPt, we examined the mechanism of cell death. It has been previously been established that rhodium metalloinsertors trigger a necrotic mechanism of cell death involving severe depletion of cellular ATP,[15] which is dependent upon DNA repair protein poly-ADP ribose polymerase (PARP).[32] Consequently, co-treatment of HCT116N HCT116O cells with rhodium metalloinsertor and an inhibitor of PARP, such as 3,4-dihydro-5[4-(1-piperindinyl)butoxy]-1(2*H*)-isoquinoline (DPQ),[33] resulted in an increase in cell viability of HCT116O cells compared to treatment with rhodium alone, essentially abolishing the differential cytotoxicity between the MMR-proficient and MMR-deficient cell lines. This result indicates that metalloinsertors induce PARP-dependent (necrotic) cell death.[15]

Here, HCT116N and HCT116O cells were treated with RhPt (20 μM) and DPQ (25 or 50 μM) for 72h, and cell viability was assayed by MTT. **Figure 3.14** (left, gray) depicts the results for the HCT116O cells, but the same results are observed in the HCT116N cell line (data not shown). DPQ alone, at either concentration, effects no change in cell viability compared to untreated cells. When cells were treated with RhPt in combination with varying concentrations of DPQ, a statistically significant *decrease* in cell viability (17% in HCT116O cells with 25 μM DPQ) is observed compared to treatment with RhPt alone, as determined by an unpaired two-tailed *t* test ($p < 0.0001$). This is in direct contrast to the previous study on rhodium metalloinsertors,[15] suggesting that RhPt cytotoxicity is PARP-independent and therefore not necrotic.

The experiment was also performed in the presence of a pan-caspase inhibitor, Z-VAD-FMK. By irreversibly binding to the active site of caspases, Z-VAD-FMK inhibits apoptosis.[34] While the previous study on metalloinsertor cytotoxicity concluded that

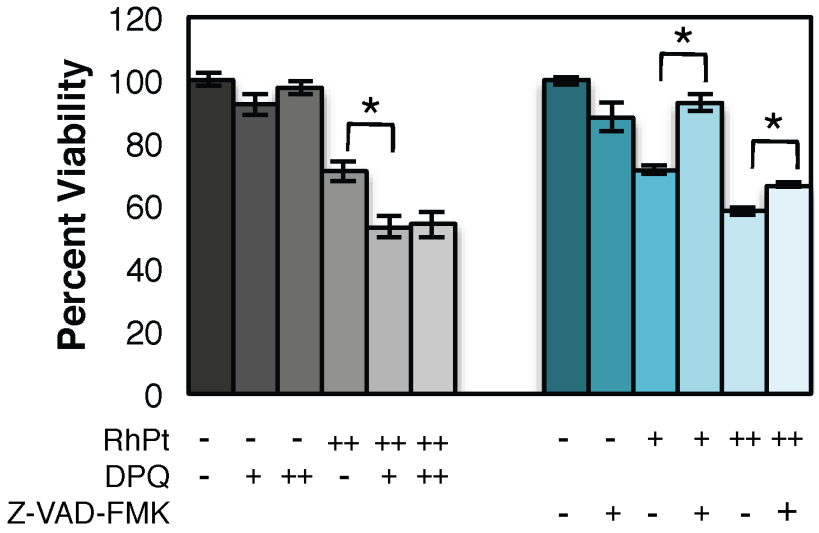


**Figure 3.14** Cell viability in HCT116O cells after 72h with PARP and caspase inhibitors. Viability is normalized to untreated controls. Left (gray): PARP inhibition assay. Cells were treated with 0 (-) or 20 μM (++) RhPt and 0 (-), 25 (+), or 50 μM (++) DPQ. DPQ does not increase the viability of cells treated with RhPt. Right (blue): Caspase inhibition assay. Cells were treated with 0 (-), 10 (+) or 20 μM (++) RhPt and 0 (-) or 20 μM (++) Z-VAD-FMK. Z-VAD-FMK increases viability in RhPt-treated cells. Addition of either inhibitor alone does not affect viability. *$p < 0.0001$(unpaired two-tailed t-test).

caspase inhibition has no effect on rhodium metalloinsertor cytotoxicity in HCT116N and HCT116O cells,[15] it is well-established that platinum complexes, namely cisplatin and oxaliplatin, typically induce apoptosis.[35,36] As such, we sought to determine whether RhPt cytotoxicity results from an apoptotic cell death mechanism.

HCT116N and HCT116O cells were treated with 0, 10, or 20 μM RhPt and either 0 or 20 μM Z-VAD-FMK for 72h. As can be seen in **Figure 3.14** (right, blue), caspase inhibition increases the viability of HCT116O cells treated with RhPt (the same results are observed with HCT116N cells). At 10 μM RhPt and 20 μM Z-VAD-FMK, cell viability is 91 ± 3%, compared to 70 ± 1% for RhPt alone, a nearly 21% increase in cell viability. At higher concentrations of RhPt (20 μM), the effects of caspase inhibition are subtler (a 7% increase in cell viability upon co-treatment with Z-VAD-FMK compared to RhPt alone), but in both cases the difference was determined to be statistically significant by unpaired two-tailed *t* test ($p < 0.0001$). These results indicate that RhPt triggers caspase-dependent, and therefore apoptotic cell death.

## 3.4 Discussion

### 3.4.1 DNA Binding Behavior

The RhPt conjugate was originally synthesized with the intention of conferring the selectivity of rhodium metalloinsertors for DNA mismatches and MMR-deficient cells to a highly potent platinum agent derived from the chemotherapeutic oxaliplatin. While selectivity was not achieved with this complex, it does exhibit its intended dual binding to DNA *via* metalloinsertion at mismatched sites and the formation of 1,2-intrastrand crosslinks at the *N*7 position of guanine residues. Additionally, the binding

affinity of the rhodium subunit at the mismatch is similar to those previously reported for rhodium metalloinsertor complexes.[14,16,17]

That RhPt performs both noncovalent metalloinsertion and covalent platinum binding establishes the bifunctionality of the conjugate (**Figure 3.15**). The lack of interplay between the rhodium and platinum binding modes suggests that each subunit functions independently and without inhibition of the other; that is, platinum binding does not alter the apparent equilibrium of metalloinsertion in the minor groove, nor does rhodium binding impede DNA platination.

### 3.4.2 Antiproliferative and Cytotoxic Activity in MMR-Deficient Cells

The antiproliferative effects of RhPt were explored in the isogenic human colorectal carcinoma cell lines HCT116N (MMR-proficient) and HCT116O (MMR-deficient) using an antibody assay for DNA synthesis.[23] RhPt exhibits antiproliferative activity similar to that of oxaliplatin and considerably outperforms cisplatin, which preferentially targets HCT116N cells. RhPt does not preferentially target either cell line. However, it is active at submicromolar concentrations, and in fact is more potent than either of its unconjugated subunits, including co-treatment with rhodium and platinum separately. The ability of RhPt to disrupt DNA synthesis was further corroborated with the *in vitro* replication assay, wherein the conjugate effectively stalls DNA replication. Furthermore, RhPt exhibits three-fold enhanced cytotoxicity over cisplatin and oxaliplatin in MMR-deficient cells, and is also substantially more potent than the Rh(Amal) and Pt(Amal) subunits. Although RhPt does not selectively inhibit proliferation of MMR-deficient cells, there is likewise no resistance – i.e., RhPt does not preferentially inhibit proliferation of MMR-*proficient* cells, and thus does not face the

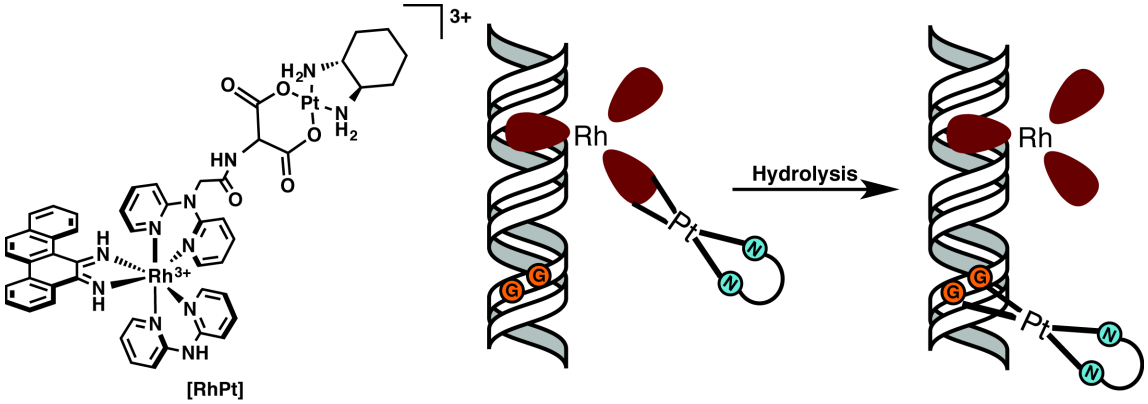


**Figure 3.15** The bifunctional DNA metalloinsertor conjugate ("RhPt"). The complex interacts with DNA through metalloinsertion at a base pair mismatch followed by formation of a covalent Pt-DNA adduct. In mismatch repair-deficient cells, RhPt exhibits enhanced cellular uptake and cytotoxicity over traditional platinum therapeutics.

same clinical limitations as cisplatin or DNA alkylating agents like MNNG.[37] The ELISA studies demonstrated that the conjugate exhibits the same anti-proliferative behavior as oxaliplatin, the first-line therapy in the treatment of late-stage colorectal cancer. Although oxaliplatin typically shows little cross-resistance with cisplatin in cell culture studies, only a modest increase in potency is observed with the MMR-deficient HCT116O cell line. As RhPt exhibits a 3 fold increase in potency over both cisplatin and oxaliplatin in this cell line, the conjugate could potentially offer another avenue for treatment of cisplatin-resistant cancers.

### 3.4.3 Cellular Uptake and Subcellular Localization of Metal Complexes

Cellular uptake was examined *via* inductively coupled plasma mass spectrometry (ICP-MS) (**Figure 3.12**). The cellular uptake of both rhodium and platinum for RhPt generally exceeds that of the monomeric complexes, with RhPt displaying high initial uptake that decreases over time, possibly due to an efflux mechanism.[38] Furthermore, the differences in uptake between RhPt and hydrolysis product Rh(Amal) suggest that the conjugate does not hydrolyze prior to entry into the cell, and is taken up in its intact form. Overall, it would appear that RhPt possesses enhanced cellular uptake properties not inherent to either subunit alone. The localization of each complex was also examined (**Figure 3.13** and **Table 3.2**). Little differentiation is observed in the subcellular distribution of the complexes, with the notable exception of a substantial increase in the nuclear rhodium concentration of RhPt compared to Rh(Amal). Curiously, this enhanced nuclear targeting of rhodium does not result in cell-selective activity.

It is likely that the enhanced potency of RhPt can be attributed largely to its increased cellular uptake properties compared to the other complexes studied in this

work. However, other than localizing to the nucleus in concentrations sufficient for DNA binding, it would appear that the subcellular localization of RhPt has little effect on its potency and does not explain its lack of cell-selectivity. This is in contrast to previous studies of monomeric rhodium metalloinsertors, wherein non-selective cytotoxicity arises from high mitochondrial rhodium content.[16,17] In the case of RhPt, the conjugate appears to hydrolyze prior to entry into the mitochondria, given that the mitochondrial rhodium content is identical to that of its hydrolysis product, Rh(Amal), while diverging substantially from mitochondrial platinum concentrations. Furthermore, the mitochondrial rhodium content is extremely low (~10 ng Rh/mg [mitochondrial protein]), while earlier studies of metalloinsetor localization have shown that cells can support an order of magnitude higher mitochondrial rhodium without losing cell-selectivity.[16,17]

### 3.4.4 Mechanism of Cell Death

To further understand the biological activity of RhPt, we examined the mechanism of cell death. It has been previously established that rhodium metalloinsertors trigger necrosis dependent upon DNA repair protein poly-ADP ribose polymerase (PARP).[15] Cytotoxicity studies revealed that the viability of cells treated with RhPt does not increase in the presence of PARP inhibitor, suggesting PARP-independent cell death. In fact, co-treatment with RhPt and PARP inhibitor is even more potent than treatment with either compound alone. This is consistent with previous studies demonstrating that inhibition of PARP can sensitize cells to *cis*-platinum through activation of the mitochondrial pathway of apoptosis, even in cell lines that are platinum-resistant.[39,40] The assay was also performed with caspase inhibitor. The viability of RhPt-treated cells increases under conditions of caspase inhibition, signifying that the conjugate triggers

caspase-dependent – and therefore apoptotic – cell death (**Figure 3.14**). This is consistent with studies of platinum cytotoxicity generally; it is well established that cisplatin and oxaliplatin typically trigger apoptosis.[35,36] This result may, in part, explain the lack of cell-selectivity observed for RhPt. By initiating apoptosis, rather than necrosis, it is possible that the highly selective biological response to mismatch recognition by rhodium is overridden by the effects of high concentrations of platinum in the cell.

Curiously, the PARP pathway appears to play vastly different roles in response to treatment with rhodium versus platinum: inhibition of the pathway in the presence metalloinsertor alone protects MMR-deficient cells from Rh-induced toxicity, while conferring synergistic cytotoxicity in the presence of a *cis*-platinum moiety. It is possible that conjugation of apoptosis-inducing *cis*-platinum (II) agents may be incompatible with the unique selectivity of metalloinsertors.

## 3.5 Conclusions

In this work, we examined the biological effects of conjugation of a DNA metalloinsertor with a platinum drug. *In vitro*, the complex successfully exhibits bifunctionality *via* dual DNA binding. In MMR-deficient cells, this strategy affords enhanced cellular uptake and potency over the individual subunits as well as versus traditional chemotherapeutics. However, RhPt is not without its limitations. The platinum subunit appears to dominate the cellular response, resulting in a loss of cell selectivity. Nevertheless, the biological analysis of RhPt provides insight into the behavior of bifunctional DNA targeting agents, as well as a foundation for the design of future conjugates that are both potent and selective in their cellular targeting.

## 3.6 References


1 Wang, D.; Lippard, S. J. *Nature Rev. Drug Discov.* **2005**, *4*, 307-320.

2 Jamieson, E. R., Lippard, S. J. *Chem. Rev.* **1999**, *99*, 2467-2498.

3 Decatris, M. P., Sundar, S., O'Byrne, K. J. *Cancer Treat. Rev.* **2004**, *30*, 53–81.

4 Fink, D.; Aebi, S.; Howell, S. B. *Clin. Cancer Res.* **1998**, *4*, 1-6.

5 Aebi, S.; Fink, D.; Gordon, R.; Kim, H. K.; Zheng, H.; Fink, J. L.; Howell, S. B. *Clin. Cancer Res.* **1997**, *3*, 1763-1767.

6 Arzimanoglou, I. I.; Gilbers, F.; Barber, H. R. K. *Cancer* **1998**, *82*, 1808-1820.

7 Lawes, D. A.; SenGupta, S.; Boulos, P. B. *Eur. J. Surg. Oncol.* **2003**, *29*, 201-212.

8 Ibrahim, A.; Hirschfeld, S.; Cohen, M. H.; Griebel, D. J.; Williams, G. A.; Pazdur, R. *The Oncologist* **2004**, *9*, 8-12.

9 Rothenberg, M. L., et al. *J. Clin. Oncol.* **2003**, *21*, 2059-2069.

10 Jackson, B. A.; Barton, J. K. *J. Am. Chem. Soc.* **1997**, *119*, 12986-12987.

11 Jackson, B. A., Barton, J. K. *Biochemistry* **2000**, *39*, 6176–6182.

12 Jackson, B. A., Alekseyev, V. Y., Barton, J. K. *Biochemistry* **1999**, *38*, 4655–4662.

13 Pierre, V. C., Kaiser, J. T., Barton, J. K. *Proc. Natl. Acad. Sci. U.S.A.* **2007**, *104*, 429–434.

14 Ernst, R. J.; Song, H.; Barton, J. K. *J. Am. Chem. Soc.* **2009**, *131*, 2359.

15 Ernst, R. J.; Komor, A. C.; Barton, J. K. *Biochemistry* **2011**, *50*, 10919-10928.

16 Komor, A. C.; Schneider, C. J.; Weidmann, A. G.; Barton, J. K. *J. Am. Chem. Soc.* **2012**, *134*, 19223-19233.

17 Weidmann, A. G.; Komor, A. C.; Barton, J. K. *Philos. Trans. R. Soc. A*. **2013**, *371*, 20120117.

18 Wisnovsky, S. P.; Wilson, J. J.; Radford, R. J.; Pereira, M. P.; Chan, M. R.; Laposa, R. R.; Lippard, S. J.; Kelley, S. O. *Chem. Biol.* **2013**, *20*, 1323-1328.

19 Muerner, H.; Jackson, B. A.; Barton, J. K. *Inorg. Chem.* **1998**, *37*, 3007-3012.

20 Gandolfi, O.; Apfelbaum, H. C.; Blum, J. *Inorg. Chim. Acta* **1987**, *135*, 27-31.

21 Kirin, S. I.; Yennawar, H. P.; Williams, M. E. *Eur. J. Inorg. Chem.* **2007**, *23*, 3686-3694.

22 Brabec, V.; Leng, M. *Proc. Natl. Acad. Sci. U.S.A.* **1993**, *90*, 5345-5349.

23 Gratzner, H. G. *Science*, **1982**, *218*, 474-475.

24 Smith, P. K.; Krohn, R. I.; Hermanson, G. T.; Mallia, A. K.; Gartner, F. H.; Provenzano, M. D.; Fujimoto, E. K.; Goeke, N. M.; Olson, B. J.; Klenk, D. C. *Anal. Biochem.* **1985**, *150*, 76-85.

25 Mosmann, T. *J. Immunol. Methods* **1983**, *65*, 55-63.

26 Li, J. J.; Kelly, T. J. *Proc. Natl. Acad. Sci. U.S.A.* **1984**, *81*, 6973-6977.

27 Liu, J.-S..; Kuo, S.-R.; McHugh, M. M.; Beerman, T. A.; Melendy, T. *J. Biol. Chem.* **2000**, *275*, 1391-1397.

28 Woynarowski, J. M.; Faivre, S.; Herzig, M. C.; Arnett, B.; Chapman, W. G.; Trevino, A. V.; Raymond, E.; Chaney, S. G.; Vaisman, A.; Varchenko, M.; Juniewicz, P. E. *Mol. Pharmacol.* **2000**, *58*, 920-927.

29 Koi, M.; Umar, A.; Chauhan, D. P.; Cherian, S. P.; Carethers, J. M.; Kunkel, T. A.; Boland, C. R. *Cancer Res.* **1994**, *54*, 4308-4312.

30 Hart, J. R., Glebov, O., Ernst, R. J., Kirsch, I. R., Barton, J. K. *Proc. Natl. Acad. Sci. U.S.A.* **2006**, *103*, 15359–15363.

31 Fujioka, A.; Terai, K.; Itoh, R. E.; Aoki, N.; Nakamura, T.; Kuroda, S.; Nishida, E.; Matsuda, M. *J. Biol. Chem.* **2006**, *281*, 8917-8926.

32 Ha, H.C., Snyder, S. H. *Proc. Natl. Acad. Sci. U.S.A.* **1999**, *96*, 13978-13982.

33 Costantino, G., Macchiarulo, A., Camaioni, E., and Pellicciari, R. *J. Med. Chem.* **2001**, *44*, 3786-3794.

34 Vandenabeele, P., Vanden Berghe, T., and Festjens, N. *Sci. STKE*, **2006**, *358*, pe44.

35 Siddik, Z. H. *Oncogene* **2003**, *22*, 7265.

36 Arango, D.; Wilson, A. J.; Shi, Q.; Corner, G. A.; Arañes, M. J.; Nicholas, C.; Lesser, M.; Mariadason, J. M.; Augenlicht, L. H. *Br. J. Cancer* **2004**, *91*, 1931.

37 Carethers, J. M.; Hawn, M. T.; Chauhan, D. P.; Luce, M. C.; Marra, G.; Koi, M.; Boland, C. R. *J. Clin. Invest.* **1996**, *98*, 199-206.

38 Eckford, P. D. W.; Sharom, F. *J. Chem. Rev.* **2009**, *109*, 2989.

39 Michels, J.; Vitale, I.; Senovilla, L.; et al. *Cell Cycle* **2013**, *12*, 877-883.

40 Sakogawa, K.; Aoki, Y.; Misumi, K.; et al. *Cancer Sci.* **2013**, *104*, 1593-1599.